Quiescent fibroblasts are protected from proteasome inhibition–mediated toxicity

Aster Legesse-Miller[a], Irene Raitman[a], Erin M. Haley[a,*], Albert Liao[a,†], Lova L. Sun[a,‡], David J. Wang[a,§], Nithya Krishnan[a], Johanna M. S. Lemons[b,‖], Eric J. Suh[a], Elizabeth L. Johnson[a], Benjamin A. Lund[a,¶], and Hilary A. Coller[a]

[a]Department of Molecular Biology and [b]Department of Chemistry, Princeton University, Princeton, NJ 08544

ABSTRACT **Proteasome inhibition is used as a treatment strategy for multiple types of cancers. Although proteasome inhibition can induce apoptotic cell death in actively proliferating cells, it is less effective in quiescent cells. In this study, we used primary human fibroblasts as a model system to explore the link between the proliferative state of a cell and proteasome inhibition–mediated cell death. We found that proliferating and quiescent fibroblasts have strikingly different responses to MG132, a proteasome inhibitor; proliferating cells rapidly apoptosed, whereas quiescent cells maintained viability. Moreover, MG132 treatment of proliferating fibroblasts led to increased superoxide anion levels, juxtanuclear accumulation of ubiquitin- and p62/SQSTM1-positive protein aggregates, and apoptotic cell death, whereas MG132-treated quiescent cells displayed fewer juxtanuclear protein aggregates, less apoptosis, and higher levels of mitochondrial superoxide dismutase. In both cell states, reducing reactive oxygen species with *N*-acetylcysteine lessened protein aggregation and decreased apoptosis, suggesting that protein aggregation promotes apoptosis. In contrast, increasing cellular superoxide levels with 2-methoxyestradiol treatment or inhibition of autophagy/lysosomal pathways with bafilomycin A1 sensitized serum-starved quiescent cells to MG132-induced apoptosis. Thus, antioxidant defenses and the autophagy/lysosomal pathway protect serum-starved quiescent fibroblasts from proteasome inhibition–induced cytotoxicity.**

Monitoring Editor
Carl-Henrik Heldin
Ludwig Institute for Cancer Research

Received: Mar 6, 2012
Revised: Jun 25, 2012
Accepted: Jul 24, 2012

INTRODUCTION

Quiescence is a cell cycle state in which cells do not actively proliferate but nevertheless retain the capacity to resume proliferation. The ability of cells to properly enter quiescence is critical for development and tissue maintenance. Quiescent cells activate a program that protects them from apoptosis, differentiation, and oxidative stress (Naderi *et al.*, 2003; Coller *et al.*, 2006; Sang and Coller, 2009; Sang *et al.*, 2008, 2010; Lemons *et al.*, 2010). Although this protected state can be beneficial for long-lived cells, the evocation of such pathways in tumor cells may allow them to survive by avoiding apoptosis or differentiation that is normally induced by anticancer agents (Sang *et al.*, 2008; Schewe and Aguirre-Ghiso, 2008).

Proliferating and quiescent cells have distinct functional requirements for protein degradation. Proliferating cells must degrade critical cell cycle regulators in a timely manner to progress though the cell cycle properly (Reed, 2006; Skaar and Pagano, 2009). In contrast, quiescent cells may use protein degradation mostly for housekeeping purposes, such as the elimination of unwanted, damaged, and old proteins to maintain cellular integrity and the reversibility of quiescence. The two major protein degradation pathways responsible for the proper turnover of proteins are the proteasome and autophagic/lysosomal pathways (Ciechanover, 2005). These two systems work in tandem to eliminate unwanted proteins and protect the organism from cellular stresses, such as reactive oxygen species

This article was published online ahead of print in MBoC in Press (http://www.molbiolcell.org/cgi/doi/10.1091/mbc.E12-03-0192) on August 8, 2012.

Present addresses: *Robert Wood Johnson Medical School, Piscataway, NJ 08854; †Philadelphia, PA 19147; ‡University of Pennsylvania, Philadelphia, PA 19104; §University of Toronto, Mississauga, ON L5L 1C8, Canada; ‖Department of Biochemistry, University of Utah, Salt Lake City, UT 84112-5650; ¶New York, NY 10005.

Address correspondence to: Hilary Coller (hcoller@princeton.edu).

Abbreviations used: Baf, bafilomycin A1; DHE, dihydroethidium; ER, endoplasmic reticulum; LC3, microtubule-associated protein 1/light chain 3; 2-ME, 2-methoxyestradiol; MnSOD, manganese superoxide dismutase; NAC, *N*-acetylcysteine; PDI, protein disulfide isomerase; PI, propidium iodide; ROS, reactive oxygen species.

(ROS)–mediated damage (Mathew *et al.*, 2007; Takeda and Yanagida, 2010; Takeda *et al.*, 2010).

The proteasome is responsible for the degradation of short-lived proteins involved in cell cycle progression, gene expression, DNA repair, apoptosis, and signal transduction, as well as abnormal and misfolded proteins (Jung *et al.*, 2009). Proteasome-mediated protein degradation involves the covalent attachment of ubiquitin to specific proteins to form Lys-48–linked polyubiquitin chains, followed by the recruitment of these proteins to the proteasome for degradation (Goldberg, 2003). The most common form of the proteasome, the 26S proteasome, consists of one 20S core particle structure (700 kDa), which contains the protease activity, and two 19S regulatory caps (900 kDa each; Voges *et al.*, 1999). There are three types of proteolytic activity within the 20S core particle: caspase-like, trypsin-like, and chymotrypsin-like activities (Heinemeyer *et al.*, 1997). Proteasome inhibitors, including MG132 (carbobenzoxy-Leu-Leu-leucinal), block the proteolytic activity of the proteasome complex (Lee and Goldberg, 1998).

Autophagy is a mechanism by which cytoplasmic material, including long-lived proteins and damaged organelles, is delivered to the lysosome for degradation (Cuervo, 2004; Yoshimori, 2004; Klionsky, 2005; Iwata *et al.*, 2006; Mathew *et al.*, 2007). During autophagy, autophagosomes form and engulf portions of the cytoplasm. Autophagosomes and lysosomes fuse, the engulfed materials are degraded, and the resulting metabolites and amino acids are recycled by the cell (Klionsky *et al.*, 2008). Autophagy is induced by nutrient limitation as a means to recover metabolites and energy; therefore this process represents a survival mechanism (Tsukada and Ohsumi, 1993; Kuma *et al.*, 2004). Autophagy may also be an important mechanism for the clearance of aggregated proteins that would otherwise be toxic to the cell (Kegel *et al.*, 2000; Ravikumar *et al.*, 2002, 2004; Komatsu *et al.*, 2006).

The inhibition of the proteasome results in many toxic effects, including the accumulation of unfolded and damaged proteins and increased levels of ROS (Fribley *et al.*, 2004; Han and Park, 2010; Han *et al.*, 2010). In response to proteasome inhibition, the cell induces specific protective mechanisms, including the unfolded protein response (Fribley *et al.*, 2004), autophagy (Milani *et al.*, 2009; Janen *et al.*, 2010), and, if the damage is severe, apoptosis (Fribley *et al.*, 2004; Ding *et al.*, 2007). In certain cases, ubiquitinated protein aggregates form juxtanuclear aggresomes that are recognized by p62/SQSTM1 (sequestosome 1). The protein p62 binds to ubiquitin via its C-terminal domain and recruits ubiquitinated protein aggregates into autophagosomes by a direct interaction with the autophagy-specific, membrane-associated protein microtubule-associated protein 1/light chain 3 (LC3; Vadlamudi *et al.*, 1996; Pankiv *et al.*, 2007). The binding of p62 to ubiquitin results in the recruitment of ubiquitinated protein aggregates to autophagosomes and their targeting for lysosomal degradation (Kegel *et al.*, 2000; Ravikumar *et al.*, 2002, 2004; Bjorkoy *et al.*, 2006; Komatsu *et al.*, 2006; Pankiv *et al.*, 2007; Kirkin *et al.*, 2009; Zheng *et al.*, 2009). Mice with a tissue-specific conditional knockout of autophagy components are deficient in the clearance of ubiquitinated protein aggregates, thereby indicating that although soluble ubiquitinated proteins can be cleared via the proteasome, aggregated, polyubiquitinated proteins are cleared by autophagy (Webb *et al.*, 2003; Komatsu *et al.*, 2005, 2006). The depletion of p62 reduces the accumulation of ubiquitinated protein aggregates in the hepatocytes and neurons of autophagy-deficient mice (Komatsu *et al.*, 2007). Thus the clearance of excess ubiquitinated proteins via autophagy has been proposed to represent an important component of the protective response to proteasome inhibition.

Recent studies have highlighted the importance of free radical generation in proteasome inhibition–mediated toxicity. Treatment of cell lines derived from a variety of tumors with proteasome inhibitors has been reported to induce apoptosis through the generation of ROS (Ling *et al.*, 2003; Fribley *et al.*, 2004; Perez-Galan *et al.*, 2006; Du *et al.*, 2009; Han and Park, 2010). Compounds that scavenge ROS or increase glutathione pools protect against proteasome inhibition-mediated apoptosis (Ling *et al.*, 2003; Fribley *et al.*, 2004; Perez-Galan *et al.*, 2006; Du *et al.*, 2009; Han and Park, 2010). However, proteasome inhibition can also result in the induction of ROS-detoxifying genes as a compensatory mechanism (Yew *et al.*, 2005; Dreger *et al.*, 2010), and in certain instances, treatment with proteasome inhibitors can protect cells from oxidative stress–induced cell death (Maher, 2008).

When multiple myeloma cells are treated with proteasome inhibitors (either MG132 or the clinically approved proteasome inhibitor bortezomib [Velcade]; Chauhan *et al.*, 2005), quiescent cells are largely resistant to the treatment and survive (Schewe and Aguirre-Ghiso, 2009). The mechanisms underlying quiescence-related resistance to proteasome inhibition may contribute to post-treatment tumor recurrence (Chauhan *et al.*, 2005). Quiescence-related resistance to proteasome inhibition in nontransformed cells has also been reported. For example, contact-inhibited quiescent normal endothelial cells are less sensitive to proteasome inhibition than proliferating cells (Drexler *et al.*, 2000); however, the underlying protective mechanism is not yet known. *Schizosaccharomyces pombe* cells in the G0 state, but not vegetative cells, respond to proteasome inhibition by activating antioxidant proteins and inducing the autophagy of mitochondria to minimize lethal ROS accumulation and cell death (Takeda *et al.*, 2010).

We observed that despite their differential protein degradation requirements, quiescent and proliferating fibroblasts maintain comparable levels of proteasome activity. Yet, quiescent fibroblasts were less sensitive to proteasome inhibition-mediated apoptosis and cell death. Therefore we were able to study populations of cells with the same underlying genetic composition but that exhibited vastly different responses to proteasome inhibition. We exploited the differential responses of proteasome-inhibited proliferating and quiescent fibroblasts to identify the critical factors that determine the functional impact of proteasome inhibition.

RESULTS

Quiescent fibroblasts are less sensitive than proliferating cells to proteasome inhibition

Primary human fibroblasts were used as a model system to study the response of proliferating and quiescent cells to proteasome inhibition. The fibroblasts were induced into quiescence using two distinct methods: contact inhibition (plating the cells in 10% serum until they became confluent) or serum starvation (sparsely plating the cells under low-serum [0.1%] conditions). Based on propidium iodide (PI) staining, both contact inhibition for 4 d (4dCI) and serum starvation for 4 d (4dSS) were shown to result in >80% of the cells with 2*N* DNA content, thereby demonstrating efficient arrest in the G1/G0 phase (Supplemental Figure S1A; Lemons *et al.*, 2010). Both 4dCI and 4dSS cells exhibited an increase in the fraction of cells with low pyronin Y and Hoechst staining, which are indicators of RNA and DNA levels. Moreover, an increase in the G0 fraction was observed and correlated with the induction of quiescence (Supplemental Figure S1B; Lemons *et al.*, 2010).

To further elucidate the responses of proliferating and quiescent fibroblasts to proteasome inhibition, the effects of known proteasome inhibitors on proliferating and quiescent fibroblasts were

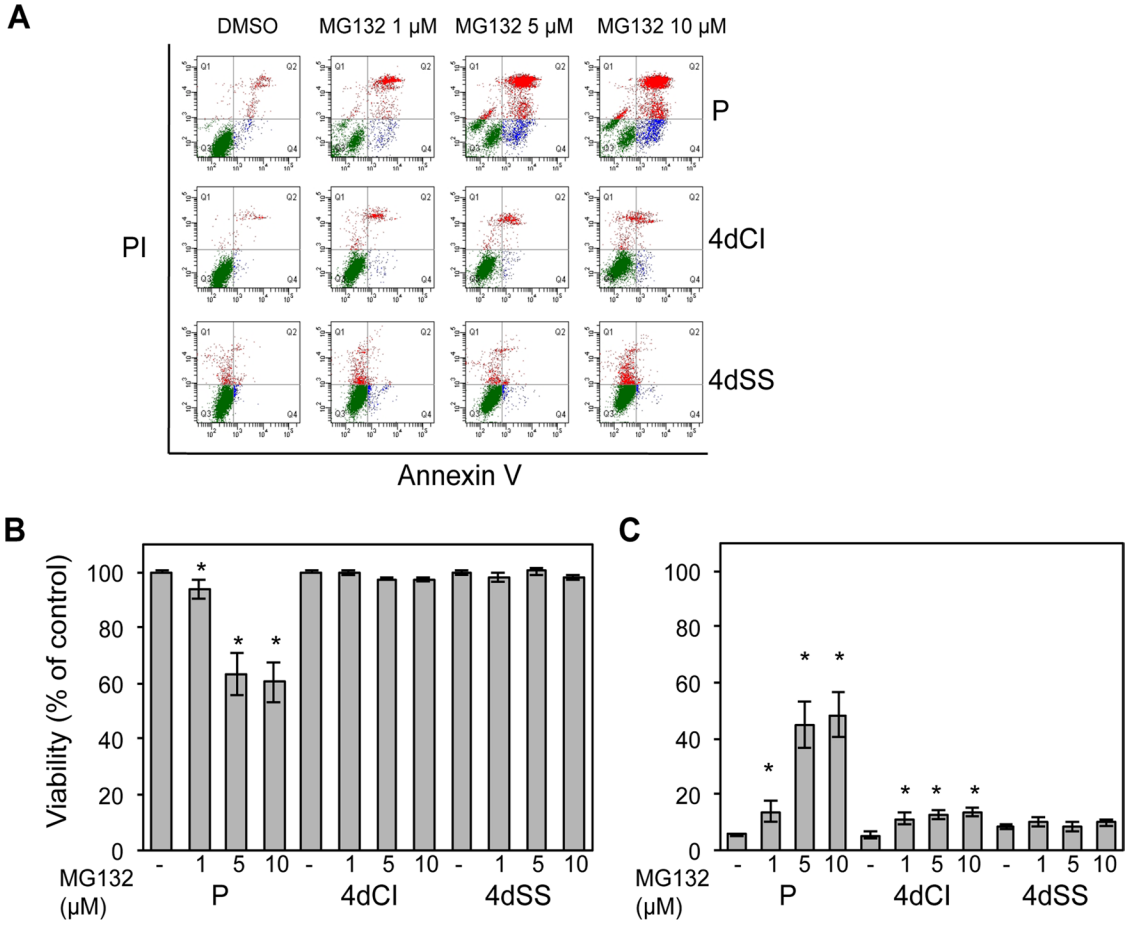

FIGURE 1: Proliferating fibroblasts are more sensitive to proteasome inhibitors than are quiescent fibroblasts. (A–C) Proliferating (P), contact-inhibited (4dCI), and serum-starved (4dSS) cells were incubated with MG132 or DMSO control, as indicated, for 24 h. Cell viability and induction of apoptosis were determined via annexin V and PI staining, followed by flow cytometry analysis. (A) Representative scatter plot of flow cytometry data. (B) Cell viability data for proteasome-inhibited and control proliferating and quiescent fibroblasts. The fraction of cells that were viable (PI negative) in the DMSO-treated cells was calibrated to 100%, and all other samples were normalized accordingly. Average viability and SE in triplicate samples from three independent experiments are shown ($n = 9$). (C) The fractions of annexin V–positive, PI-negative (early apoptotic) cells, annexin V– and PI-positive (late apoptotic) cells, annexin V–negative, PI-positive (very late apoptotic or necrotic) cells. The average and SE for three independent experiments, each performed in triplicate ($n = 9$), are shown. Asterisks indicate a statistically significant difference ($p < 0.05$) between MG132-treated and control cells.

examined. The induction of apoptosis and cell death was monitored using the apoptotic marker annexin V and the cell viability marker PI. A representative flow cytometry scatter plot is presented in Figure 1A. Treatment with either MG132 or epoxomicin for 24 h resulted in a statistically significant, dose-dependent decrease in proliferating cell viability based on the fraction of cells negative for PI (Figure 1B and Supplemental Figure S2A). In contrast, quiescent cells maintained high viability at 24 h even at concentrations of proteasome inhibitors that reduced the viability of proliferating cells by almost 50% (10 μM for MG132, 1 μM for epoxomicin; Figure 1B and Supplemental Figure S2A).

After 24 h of treatment with MG132, proliferating cells exhibited a significant increase in annexin V and PI staining. At the highest dose (10 μM), ~50% of proliferating cells were apoptotic (in Figure 1A, the lower right [Q4], upper right [Q2], and upper left [Q1] quadrants represent early apoptosis, late apoptosis, and very late apoptosis or necrosis, respectively). In comparison, quiescent fibroblasts were largely unaffected by MG132 treatment, showing far lower levels of apoptosis. At the highest dose of MG132, ~14% of the contact-inhibited fibroblasts and 10% of the serum-starved fibroblasts exhibited signs of apoptosis (Figure 1C). Even after 48 h of MG132 treatment, a significantly higher number of quiescent fibroblasts maintained viability than proliferating fibroblasts (Supplemental Figure S2B).

Proliferating fibroblasts accumulate in the G2/M phase in response to MG132 treatment

We hypothesized that a certain extent of the differential response of proliferating and quiescent fibroblasts to proteasome inhibition may stem from a need for the proteasome-dependent elimination of molecules that facilitate progression through the cell cycle, such as cyclin B or securin in proliferating fibroblasts (Brandeis and Hunt, 1996; Gordon *et al.*, 1996; Huo *et al.*, 2006). To assess the effects of proteasome inhibition on cell cycle progression, we used

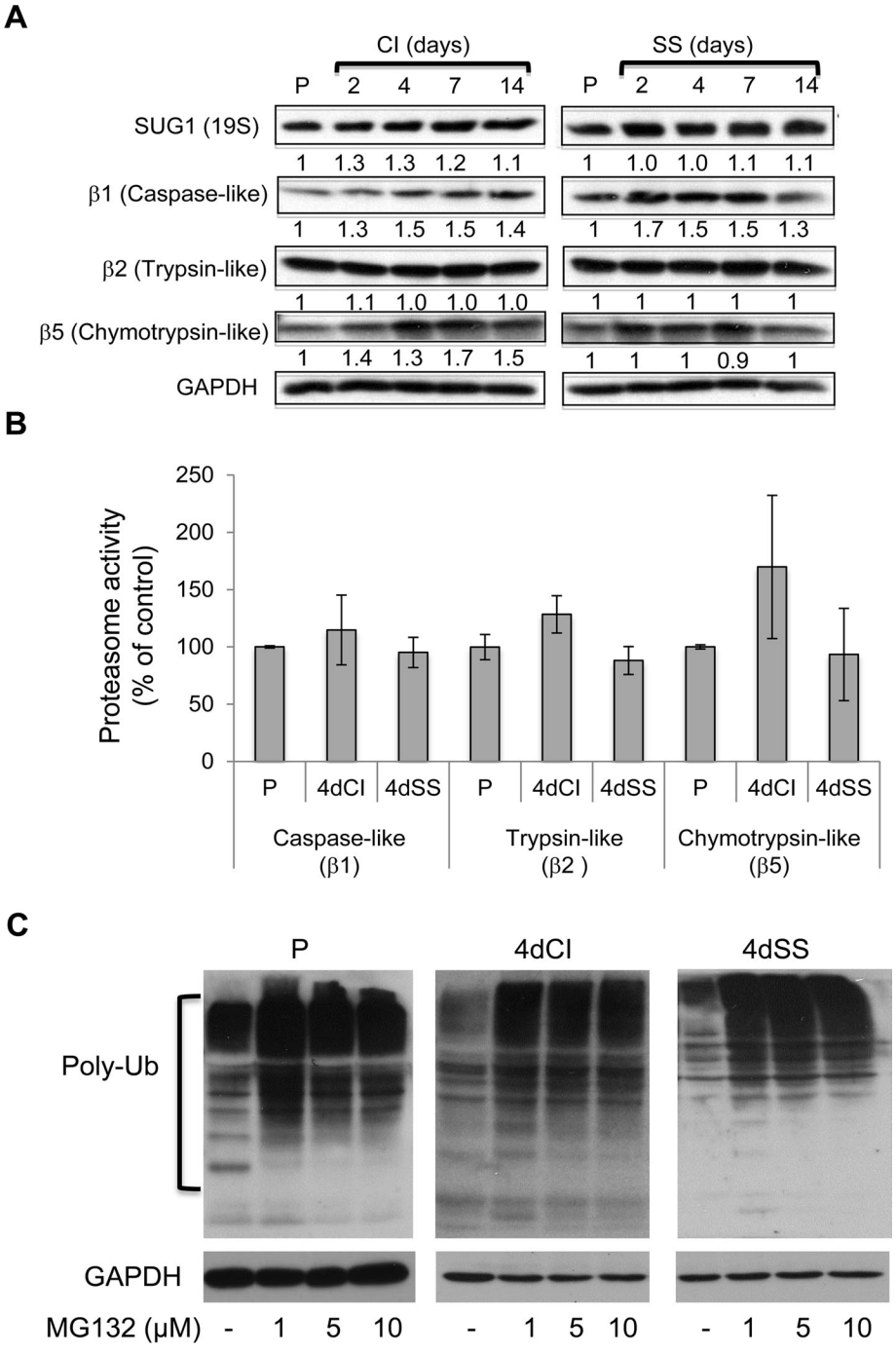

FIGURE 2: Proteasome levels and activity are comparable in proliferating and quiescent fibroblasts. (A) Protein lysates from fibroblasts induced into quiescence by contact inhibition or serum starvation were collected at the indicated time points. Constitutive proteasome subunit levels were monitored by immunoblotting. GAPDH was used as a loading control. The ratio of the proteasome subunit to GAPDH, normalized to the proliferating (P) sample, is shown. (B) Total proteins from proliferating (P), contact-inhibited (4dCI), and serum-starved (4dSS) cells were collected, and 20S proteasome activity was monitored using fluorescent substrates for the indicated enzymes. Enzyme activity of the proliferating sample was calibrated to 100% for each enzyme, and the other samples were normalized accordingly. Average fluorescence and standard deviations in triplicate samples from two independent experiments ($n = 6$) are shown. (C) Cells were treated with MG132 as indicated for 24 h, and the accumulation of ubiquitinated proteins was monitored by immunoblotting. GAPDH was used as a loading control.

flow cytometry to compare the fraction of MG132-treated and dimethyl sulfoxide (DMSO)–treated proliferating fibroblasts in different phases of the cell cycle 24 h after treatment. MG132 treatment resulted in a significant accumulation of cells in the G2/M phase (55% of MG132-treated cells vs. 11% of DMSO-treated cells; Supplemental Figure S2C). Similarly, treatment of proliferating cells with lactacystin, another proteasome inhibitor, also resulted in an accumulation of cells in the G2/M phase (unpublished data).

The cyclin-dependent kinase inhibitor $p21^{Cip1}$, a protein degraded by the proteasome, accumulated to relatively high levels in response to proteasome inhibition, thereby suggesting that proliferating fibroblasts were likely affected by checkpoint arrest (Dulic *et al.*, 1998; Tamura *et al.*, 2010; Supplemental Figure S2D). Thus proteasome inhibition–mediated apoptosis in proliferating fibroblasts likely does not reflect only the mechanics of cell cycle progression. Moreover, the higher level of resistance exhibited by serum-starved fibroblasts relative to contact-inhibited fibroblasts (Figure 1), even though both cell types were cell cycle-arrested and robustly accumulated $p21^{Cip1}$ (Supplemental Figures 1 and 2D), suggests that additional protective mechanisms are involved.

Proteasome levels and activity are comparable in proliferating and quiescent fibroblasts

The quiescence-related resistance to proteasome inhibition–mediated apoptosis and cell death may reflect a decreased reliance on proteasome-mediated protein degradation and/or activation of survival mechanisms in quiescent fibroblasts. Proliferating fibroblasts are expected to rely heavily on the proteasome for rapid protein turnover during cell cycle progression. To compare proteasome activities in proliferating and quiescent fibroblasts, we used immunoblotting to monitor the levels of proteins within the constitutive 26S proteasome subunits. The levels of 26S subunits—β1, β2, and β5 20S, which are responsible for caspase-like, trypsin-like, and chymotrypsin-like activity, respectively—and the 19S ATPase SUG1 were monitored in proliferating and quiescent cells (quiescence was induced by contact inhibition or serum starvation for 2, 4, 7, and 14 d). The levels of β1, β5, and SUG1 subunits were slightly elevated in contact-inhibited quiescent cells relative to proliferating cells, whereas β2 subunit levels were unchanged (Figure 2A). Serum-starved quiescent cells exhibited slightly elevated β1 subunit levels and showed no significant change in the levels of the other subunits relative to proliferating cells. Thus the induction of quiescence in primary fibroblasts does not appear to be associated with significant changes in proteasome levels.

Proteasome activity was measured in cell lysates prepared from proliferating and quiescent cells using three fluorogenic 20S proteasome substrates, one specific for each of the caspase-like, trypsin-like, and chymotrypsin-like activities. Caspase-like (β1), trypsin-like (β2), or chymotrypsin-like (β5) activity was consistent in all lysates from contact-inhibited fibroblasts (β1 = 114 ± 30%, β2 = 128 ± 5.8%, and β5 = 169 ± 62% relative to proliferating lysate; Figure 2B). Lysates from serum-starved fibroblasts also exhibited no significant changes in overall proteasome activity (β1 = 95 ± 13%, β2 = 88 ± 11%, and β5 = 93 ± 40% relative to proliferating lysates). Thus the overall proteasome activities are not significantly different in quiescent (4dSS or 4dCI) and proliferating fibroblasts.

The accumulation of ubiquitinated proteins in MG132-treated proliferating and quiescent fibroblasts was monitored as an indicator of in vivo proteasome activity using immunoblotting. Proliferating, contact-inhibited, and serum-starved cells were incubated for 24 h in the presence of increasing concentrations of MG132, and ubiquitinated protein accumulation was monitored using an antibody that recognizes monoubiquitinated and polyubiquitinated proteins (Figure 2C). Quiescent and proliferating fibroblasts contained similar baseline levels of ubiquitinated proteins and exhibited similar increases in ubiquitinated proteins in response to proteasome inhibition (Figure 2C). Thus, based on immunoblotting for proteasome subunits, in vitro proteasome activity assays, and the accumulation of ubiquitinated proteins within proteasome-inhibited fibroblasts, we conclude that the differential utilization of proteasome pathways or overall accumulation of ubiquitinated proteins is unlikely to explain why quiescent cells are less sensitive to proteasome inhibition–mediated cell death. Because quiescent cells remain viable despite a significant accumulation of ubiquitinated proteins, a different pathway must maintain the viability of proteasome-inhibited quiescent cells.

Proliferating and quiescent fibroblasts induce autophagy in response to proteasome inhibition

We sought to determine the mechanisms by which quiescent fibroblasts remain viable despite proteasome inhibition. Several studies have reported that autophagy serves as a survival mechanism in cells treated with proteasome inhibitors (Milani *et al.*, 2009) and that autophagy is induced in both serum-starved and contact-inhibited quiescent cells (Valentin and Yang, 2008). We hypothesized that autophagy might play a role in protecting quiescent fibroblasts from proteasome inhibition–mediated cell death.

To test this hypothesis, we monitored the levels of an autophagy-specific form of the LC3 protein, LC3 II, compared with a housekeeping protein (Klionsky *et al.*, 2008). A time-dependent increase in the ratio of LC3 II to glyceraldehyde-3-phosphate dehydrogenase (GAPDH) was observed as cells were induced into quiescence by serum starvation or contact inhibition (Figure 3A). Consistent with published data, these results confirm the induction of autophagy in both contact-inhibited and serum-starved primary fibroblasts (Valentin and Yang, 2008). We describe more fully the induction of autophagy with contact inhibition elsewhere (Haley, Raitman, Suh, Krishnan, Zhang, Cho, Guo, Evertts, Lund, Lemons, and Coller, unpublished data).

Although proliferating fibroblasts exhibit low baseline levels of autophagy, previous studies suggested that autophagy can be induced in response to proteasome inhibition (Zhu *et al.*, 2010; Kawaguchi *et al.*, 2011). We observed an increase in the ratio of LC3 II to GAPDH in response to MG132 treatment for cells in proliferating, contact-inhibited, and serum-starved states (Figure 3B). To test whether the high levels of LC3 II in quiescent cells in response to MG132 treatment result from a blockade of autophagy degradation or from active flux through the pathway, we monitored LC3 II levels in proliferating and quiescent fibroblasts treated with MG132 in the presence or absence of bafilomycin A1 (Baf). Baf is a vacuolar-type H(+)-ATPase pump inhibitor that prevents lysosomal-mediated degradation. Baf treatment also blocks the fusion of autophagosomes with lysosomes (Yoshimori *et al.*, 1991; Yamamoto *et al.*, 1998) due to an increase in the lysosomal pH (Yoshimori *et al.*, 1991), which inhibits autophagy (Yamamoto *et al.*, 1998). Baf-treated proliferating and quiescent cells exhibited an increase in the ratio of LC3 II to GAPDH. For proliferating and contact-inhibited cells, Baf treatment in conjunction with MG132 treatment led to a further increase in the ratio of LC3 II to GAPDH compared with MG132 treatment alone (Figure 3C). In comparison, in serum-starved cells, Baf treatment combined with MG132 treatment did not change the ratio of LC3 II to GAPDH compared with MG132 treatment alone. These results indicate that MG132 treatment results in active autophagic flux in proliferating and contact-inhibited primary fibroblasts (Figure 3C).

Bafilomycin A1 sensitizes serum-starved fibroblasts to proteasome inhibition–mediated apoptosis

To evaluate further the functional role of the autophagy/lysosomal pathway in response to proteasome inhibition in proliferating and quiescent cells, we monitored the effect of Baf on proteasome inhibition–mediated induction of apoptosis. Apoptosis induction was assessed by monitoring caspase 3/7 activity using a luminescent caspase substrate. This assay is optimized for high-throughput screening in 96-well plates and allows multiple concentrations and combination of drugs to be tested in triplicate at different time points. Because there are a large number of cells within each well of contact-inhibited cells, a significant increase in caspase 3/7 activity may represent only a small fraction of all of the cells within that well, and thus the data for contact-inhibited cells are difficult to interpret. Therefore, this assay was used to compare proliferating and serum-starved cells only. Changes in caspase 3/7 activity were examined in proliferating and serum-starved cells treated with increasing concentrations of MG132 (0–10 μM) in the presence or absence of 100 nM Baf. MG132 treatment resulted in dose-dependent increases in caspase 3/7 activity (Figure 3D), thereby indicating the induction of apoptosis. Baf treatment strongly enhanced MG132-induced apoptosis in serum-starved fibroblasts but had no significant effect on proliferating fibroblasts at 48 h posttreatment. A slight reduction in caspase 3/7 activity was observed in proliferating cells at 24 h posttreatment. The induction of apoptosis in serum-starved fibroblasts at 48 h posttreatment with 10 μM MG132 more than doubled in the presence of Baf. Similar results were also observed for bortezomib, a potent and specific proteasome inhibitor that is clinically approved for the treatment of multiple myeloma (Hideshima *et al.*, 2001), mantle cell lymphoma (Goy *et al.*, 2005), and other solid tumors. As observed for the MG132 treatment (Figure 3D), the induction of apoptosis was relatively low in serum-starved fibroblasts compared with proliferating fibroblasts treated with bortezomib (Supplemental Figure S3). However, after 72 h of treatment, the proliferating cells were dead, and the combination of bortezomib and Baf had a strong synergistic apoptotic effect in serum-starved cells. The treatment of proliferating fibroblasts with Baf led to reduced bortezomib-induced caspase 3/7 activity at 24 h posttreatment but had little effect after 48 h (Supplemental Figure S3). Thus, by using two proteasome inhibitors—MG132 and bortezomib—we showed that Baf has a strong, synergistic apoptotic effect on serum-starved fibroblasts.

To further assess the functional role of autophagy with respect to the viability of proteasome-inhibited quiescent cells, we transduced proliferating and quiescent fibroblasts with a retroviral vector containing a short hairpin RNA (shRNA) against beclin-1, a critical

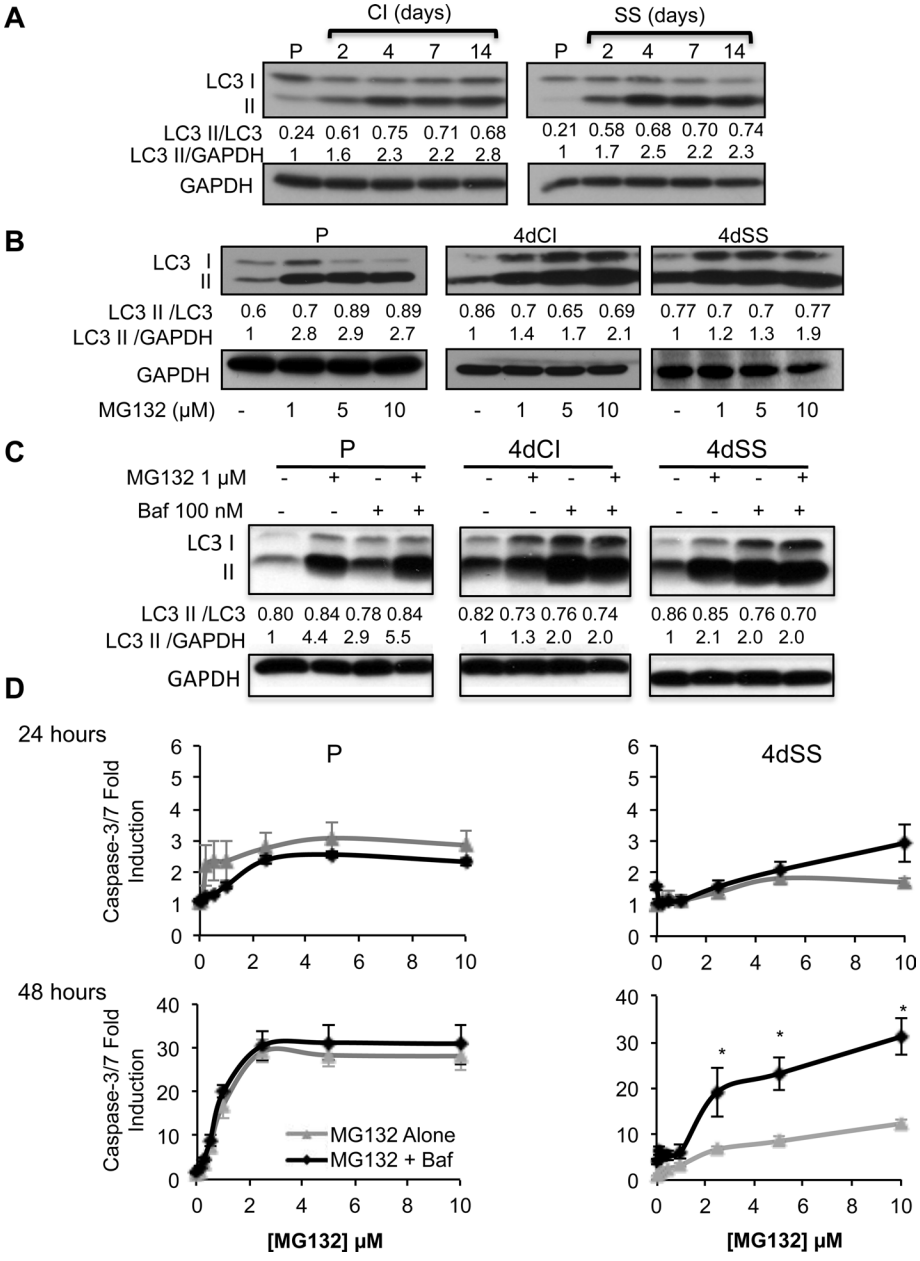

FIGURE 3: Inhibition of autophagy results in increased apoptotic cell death in proteasome-inhibited, serum-starved fibroblasts. (A) Autophagy is induced in contact-inhibited (CI) and serum-starved (SS) fibroblasts. Protein lysates were collected as in Figure 2A and subjected to immunoblot analysis with an antibody to LC3. The ratio of LC3 II to total LC3 (LC3 I + LC3 II) is shown, as well as the ratio of LC3 II to GAPDH, normalized to the proliferating sample. (B) MG132 treatment leads to induction of autophagy in proliferating and quiescent cells. Cells were treated with increasing amounts of MG132 for 24 h, and LC3 levels were monitored by immunoblot analysis. The ratios of LC3 II to total LC3 and LC3 II to GAPDH, normalized to DMSO (–) control, are shown. (C) MG132 treatment leads to active autophagy flux. Cells were treated for 24 h with DMSO (–), MG132, Baf, or MG132 and Baf, as indicated. LC3 levels were monitored by immunoblot analysis. The ratios of LC3 II to total LC3 and of LC3 II to GAPDH normalized to DMSO-treated control cells are shown. (D) Treatment with Baf sensitizes serum-starved fibroblasts to MG132. Proliferating and 4dSS fibroblasts were treated with MG132 (0–10 μM) in the presence or absence of 100 nM Baf for 24 and 48 h. Caspase 3/7 activity was monitored using a luminescent substrate. The fold change of caspase 3/7 activity in MG132-treated compared with DMSO-treated cells is shown. The experiments were performed three times in triplicate; mean fold change and SE are shown ($n = 9$). Asterisks indicate a significant difference for cells treated with MG132 together with 100 nM Baf compared with cells treated with MG132 alone at the same concentration ($p < 0.05$).

upstream regulator of autophagy responsible for mediating the initial stages of autophagosome formation (Cao and Klionsky, 2007). Immunoblot analysis confirmed beclin-1 depletion of >80% in shbeclin-1–transduced fibroblasts in all cell states (Supplemental Figure S4A). Beclin-1 knockdown resulted in a modest increase in caspase 3/7 activity in MG132-treated proliferating fibroblasts but had little impact on apoptosis in serum-starved fibroblasts (Supplemental Figure S4B). Because beclin-1 knockdown and Baf inhibit different stages of autophagy via the inhibition of autophagosome formation or the fusion of autophagosomes and lysosomes, respectively, these results suggest that autophagosome formation may be more important in proliferating cells, whereas autophagy/lysosomal activity may be more important in serum-starved cells. Taken together, these results suggest that autophagy/lysosomal pathways may protect serum-starved fibroblasts from proteasome inhibition–mediated apoptosis and cell death.

Microarray analysis reveals a strong transcriptional response to MG132 treatment in proliferating and quiescent fibroblasts

To gain insight into the molecular mechanisms that contribute to the resistance of quiescent fibroblasts to MG132 treatment, microarray analysis was performed to assess the global transcriptional response to MG132 treatment in proliferating and quiescent fibroblasts. Proliferating, contact-inhibited, and serum-starved fibroblasts were treated with DMSO (as a vehicle control), 1 μM MG132, 100 nM Baf, or both MG132 and Baf for 24 h. These treatment concentrations were selected to minimize cell death in all proliferative states. RNA was collected from each sample, fluorescently labeled, and hybridized to whole–human genome microarrays. For each cell state, cells treated with DMSO were compared with cells treated with MG132, Baf, or both (see *Materials and Methods* for details). A total of 6786 genes were identified that exhibited at least a twofold change in expression in at least one array. Based on their expression profiles, genes were clustered into 10 groups using the *K*-means algorithm. The genes in each cluster are listed in Supplemental Table S1, and a heat map displaying the results is shown in Figure 4.

For all cell cycle states, MG132 treatment, either alone or combined with Baf, resulted in the strongest signal (i.e., induction or repression) in the microarray data. MG132-induced genes (clusters 1 and 8 in

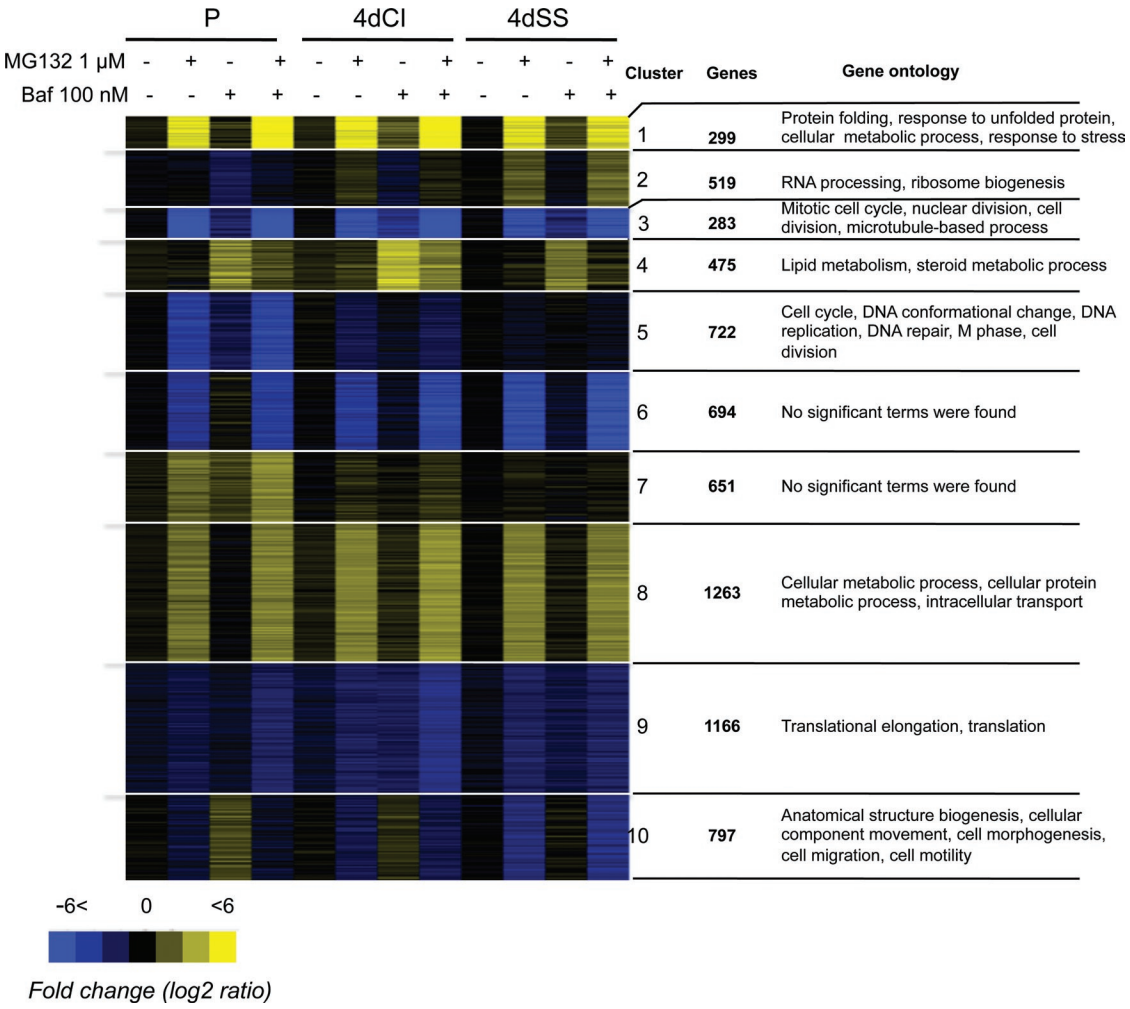

FIGURE 4: MG132 treatment results in a widespread transcriptional response for both proliferating and quiescent cells. Proliferating (P), contact-inhibited (4dCI), or serum-starved (4dSS) fibroblasts were treated as indicated for 24 h. From each sample, RNA was collected, fluorescently labeled, and hybridized to whole–human genome microarrays. For each sample, the $\log_2$ of the ratio of expression relative to the DMSO-treated control is shown. The gene expression profile was used to cluster the genes into 10 groups using *K*-means clustering. Yellow indicates high expression, and blue indicates low expression.

Figure 4) were enriched in genes encoding heat shock proteins, chaperones involved in protein folding ($p < 2.3 \times 10^{-7}$ by Gene Ontology Term Finder analysis), proteasome subunits, and proteins involved in autophagy. MG132-repressed genes (clusters 3, 5, 6, and 9 in Figure 4) were enriched in genes encoding proteins involved in protein translation (cluster 9, $p < 5 \times 10^{-4}$), likely reflecting a compensatory reaction to elevated protein levels, and were also enriched in genes annotated to the mitotic cell cycle (cluster 3, $p < 1.6 \times 10^{-5}$) and cell cycle progression (cluster 5, $p < 10^{-8}$), which may reflect MG132-induced cell cycle arrest. The transcriptional response to Baf treatment (cluster 4 in Figure 4) showed an enrichment for genes encoding proteins that participate in lipid metabolism and sterol biosynthesis ($p < 3.3 \times 10^{-6}$), which likely reflects the inability of these cells to recycle their membranes.

Thus the transcriptional response to proteasome inhibition includes the up-regulation of transcripts encoding proteins involved in autophagy and proteasome-mediated protein degradation, presumably to compensate for the MG132-mediated impairment of protein degradation. For all cell cycle states, treatment with MG132 also resulted in the transcriptional induction of multiple regulators of the cellular redox state, including the mitochondrially localized manganese superoxide dismutase (MnSOD) discussed later (clusters 8 and 1 in Figure 4, respectively; Supplemental Table S1).

Proliferating and quiescent fibroblasts induce chaperones in response to proteasome inhibition

One of the protective responses activated by cells treated with proteasome inhibitors is to increase the levels of chaperones to prevent aggregation and promote folding (Bush *et al.*, 1997; Mathew and Morimoto, 1998; Sherman and Goldberg, 2001). Our microarray data revealed that transcripts encoding chaperones that localize to the cytoplasm, mitochondria, and endoplasmic reticulum (ER) were among the transcripts that were most strongly induced in response to MG132 treatment. Hsp90, Hsp40, and Hsp70 were induced in response to MG132 at the transcript level in all cell cycle states (Figure 4, cluster 1; Supplemental Table S1). The effect of proteasome inhibition on chaperone protein levels was further examined. MG132 treatment resulted in ~20-fold

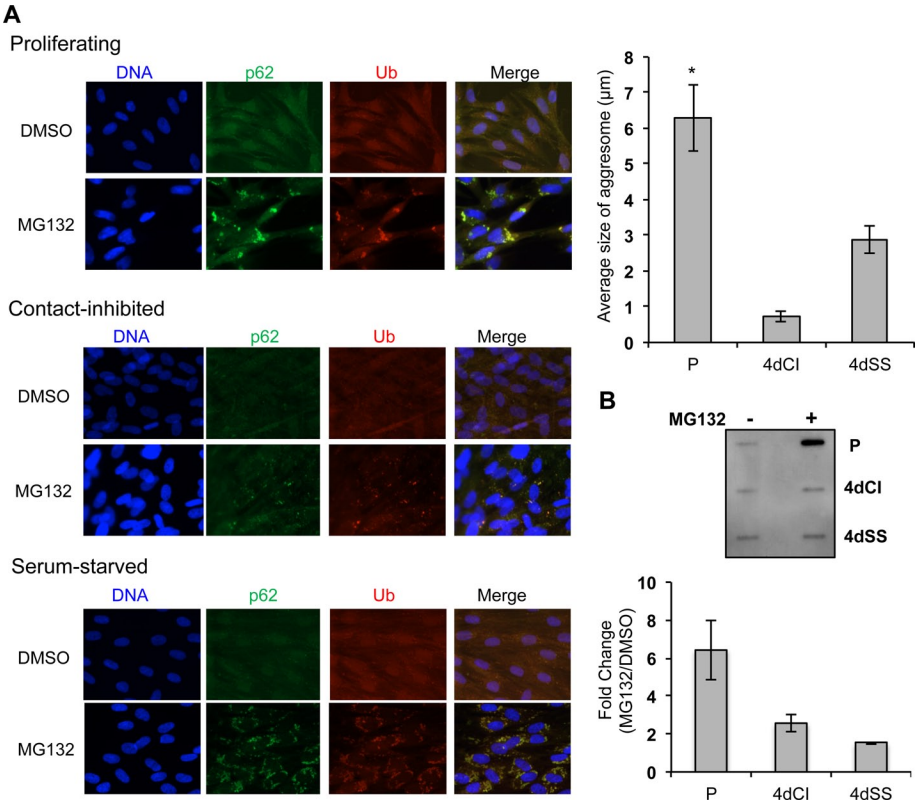

FIGURE 5: Proteasome-inhibited quiescent fibroblasts exhibit less accumulation of ubiquitin- and p62-positive juxtanuclear aggregates. (A) Fibroblasts were plated on chamber slides under proliferating (top), contact-inhibited (middle), or serum-starved (bottom) conditions and treated with DMSO as vehicle control or MG132 (1 μM) for 24 h. Samples were fixed and stained with primary antibodies to ubiquitin and p62. Fluorescent secondary antibodies (Alexa 488 for p62 and Alexa 633 for ubiquitin) were used for visualization. Samples were stained with Hoechst to visualize DNA. Images were taken at 40× magnification. Volocity software was used to measure the average aggresome length in images of proliferating and quiescent cells from two different experiments (six images were used for proliferating, four images for contact-inhibited, and five images for serum-starved cells). Asterisk indicates a statistically significant difference between P and 4dCl and between P and 4dSS ($p < 0.05$). (B) Total proteins were prepared in the presence of 1% SDS, and the samples were filtered through a 0.2-μm-pore-size cellulose acetate membrane. Protein aggregates retained by the cellulose acetate membrane were visualized by Western blot analysis with anti-ubiquitin antibody (top). ImageJ software (National Institutes of Health, Bethesda, MD) was used to quantify ubiquitinated protein levels for each sample in two independent experiments, and the fold change of ubiquitinated proteins comparing MG132-treated to the DMSO control samples is plotted (bottom). Error bars, SD. *p* value for proliferating vs. 4dSS is 0.052.

induction of Hsp70 in both proliferating and quiescent cells. In comparison, cytoplasmic heat shock protein hsp90 and mitochondrial heat shock protein hsp60 were similarly expressed in proliferating and quiescent cells and were moderately induced in response to MG132 treatment (Supplemental Figure S5).

Unfolded proteins are shuttled from the ER to the cytoplasm for proteasomal degradation (Maattanen *et al.*, 2010). Proteasome inhibition leads to an accumulation of unfolded proteins in the ER, which in turn leads to ER stress (Lee *et al.*, 2003; Fribley *et al.*, 2004). In an attempt to reduce the amount of misfolded proteins in the ER, cells induce the production of ER chaperones that promote protein folding. Our analysis of the expression of ER-resident chaperones, such as Bip, calnexin, and protein disulfide isomerase (PDI), revealed that Bip levels were similar in proliferating and quiescent fibroblasts and were not strongly induced by proteasome inhibition (Supplemental Figure S5). Moreover, calnexin and PDI levels were also similar in proliferating and quiescent fibroblasts and were not induced by MG132 treatment (Supplemental Figure S5). Therefore, although chaperone induction in the cytoplasm, mitochondria, and ER may, in general, represent an important part of the protective response to proteasome inhibition, further investigation is needed to determine whether these chaperones play specific roles in the relative resistance of quiescent fibroblasts to proteasome inhibition–induced cell death.

Proteasome-inhibited quiescent fibroblasts exhibit a decreased accumulation of ubiquitin- and p62-positive juxtanuclear aggregates

Although the responses of proteasome-inhibited proliferating and quiescent fibroblasts are similar in many respects, immunofluorescence studies revealed a difference in the intracellular localization of ubiquitinated proteins. In MG132-treated proliferating fibroblasts, ubiquitinated proteins were localized to large juxtanuclear protein aggregates that also contained p62/SQSTM1 (Bjorkoy *et al.*, 2005; Pankiv *et al.*, 2007; Figure 5A). In contrast, MG132-treated, contact-inhibited fibroblasts exhibited small ubiquitin- and p62-positive foci that were dispersed throughout the cytoplasm. In MG132-treated, serum-starved fibroblasts, the ubiquitin- and p62-positive foci were larger than in contact-inhibited fibroblasts and more likely to be found in dispersed aggregates rather than the localized aggregates found in proliferating fibroblasts. Indeed, measurement of aggresome size using Volocity software revealed that although proteasome inhibition led to an accumulation of ubiquitinated proteins in proliferating cells comparable with that in quiescent cells (Figure 2C), the average aggresome size was higher in proliferating (6.3 ± 0.94 μm) cells than serum-starved (2.9 ± 0.15 μm) and contact-inhibited (0.7 ± 0.39 μM) cells (Figure 5A). In addition, we measured cellular aggresome levels based on the fact that proteins in aggresomes become insoluble in the presence of detergent. We found fewer detergent-insoluble aggregated proteins in quiescent cells compared with proliferating cells in response to proteasome inhibition (Figure 5B). This result is consistent with relatively dispersed, smaller ubiquitinated protein aggregates in quiescent cells. Therefore, we conclude that proteasome-inhibited fibroblasts contain comparable amounts of ubiquitinated proteins, but the extent of aggregation and localization is dependent on the proliferative status of the cell.

To further test the contribution of ubiquitin-positive protein aggregates to proteasome inhibition-mediated apoptosis, we used an shRNA to knock down p62, which has been reported to be required for formation of aggresome-like structures and to facilitate degradation of ubiquitinated protein aggregates by autophagy (Bjorkoy *et al.*, 2005; Pankiv *et al.*, 2007). Indeed, our experiments showed significantly decreased aggregation of ubiquitinated proteins in proliferating and serum-starved,

MG132-treated p62-knockdown fibroblasts compared with fibroblasts with intact p62 (Figure 6A). After 24 h, p62 knockdown in the proliferating cells resulted in a moderate but significant reduction of apoptosis compared with cells transduced with the shRNA control (Figure 6C). Thus, decreased levels of p62 resulted in reduced ubiquitinated protein aggregation and less apoptosis, suggesting that protein aggregation may contribute to the early apoptotic response of proliferating fibroblasts to proteasome inhibition.

N-Acetylcysteine protects fibroblasts from MG132-induced protein aggregation and apoptosis

Proteasome inhibition-mediated apoptosis has been shown to be associated with free radical generation in several cancer cell lines (Ling *et al.*, 2003; Fribley *et al.*, 2004; Perez-Galan *et al.*, 2006; Du *et al.*, 2009), and increased ROS levels have been reported to induce aggresome formation (Marambio *et al.*, 2010). We tested the effects of the glutathione precursor and antioxidant *N*-acetylcysteine (NAC) on MG132-induced, intracellular, ubiquitin-positive aggregates and the extent of apoptosis. Proliferating, contact-inhibited, and serum-starved fibroblasts were treated with 1 μM MG132 and 2 mM NAC for 24 h, and the accumulation of ubiquitin- and p62-positive aggregates was examined by immunofluorescence. Immunofluorescence studies revealed that the addition of NAC to MG132-treated cells significantly reduced the number of ubiquitin-positive aggregates in proliferating and serum-starved cells based on Volocity software quantification (Figure 7A, right), consistent with a role for ROS in protein aggregation. NAC treatment also significantly reduced the extent of MG132-induced apoptosis in proliferating and serum-starved fibroblasts (Figure 7B). These results reinforce the importance of ROS in proteasome inhibition–mediated apoptosis (Ling *et al.*, 2003; Fribley *et al.*, 2004; Perez-Galan *et al.*, 2006; Du *et al.*, 2009).

Treatment with MG132 increases cellular superoxide levels in proliferating cells, and treatment with 2-methoxyestradiol sensitizes serum-starved quiescent fibroblasts to proteasome inhibition

Other researchers have reported that there is a correlation between proliferative status and sensitivity to oxidative stress in human fibroblasts (Naderi *et al.*, 2003). Our microarray analysis revealed that treatment with MG132 resulted in the induction of multiple free radical–detoxifying gene products, including the mitochondrially localized manganese superoxide dismutase, MnSOD, an enzyme that catalyzes the conversion of superoxide into oxygen and hydrogen peroxide (Figure 8A). Although MG132 treatment induced MnSOD expression in both proliferating and quiescent cells, contact-inhibited and serum-starved cells showed a greater change in MnSOD transcript expression compared with proliferating fibroblasts (Figure 8A). A Western blot analysis was used to monitor the levels of the ROS-detoxifying enzymes MnSOD and catalase, an enzyme that converts hydrogen peroxide to water and oxygen. The protein concentrations of MnSOD and catalase were higher in quiescent fibroblasts than in proliferating cells (Figure 8B), consistent with a previous report (Sarsour *et al.*, 2008). MG132 treatment further elevated MnSOD levels in both proliferating and quiescent fibroblasts. We hypothesized that the higher levels of ROS-detoxifying enzymes in quiescent fibroblasts contributes to the protection of quiescent fibroblasts from proteasome inhibition–induced apoptosis. We monitored intracellular superoxide levels using dihydroethidium (DHE), an indicator of superoxide anions. As shown in Figure 8C, proteasome inhibition led to significant induction of superoxide levels in proliferating cells, whereas quiescent cells maintained basal superoxide levels even during proteasome inhibition. These results suggest a possible role for ROS homeostasis mechanisms in quiescent fibroblasts in response to proteasome inhibition.

We hypothesized that an improved ability to detoxify free radicals may protect quiescent fibroblasts from proteasome inhibition–mediated apoptosis. To test this, we treated proliferating and serum-starved fibroblasts with 2-methoxyestradiol (2-ME) in the presence of increasing concentrations of MG132 and monitored the induction of apoptosis. 2-ME treatment has been shown to increase cellular superoxide levels in a manner similar to superoxide dismutase inhibition; however, the exact mechanism is not clear (Huang *et al.*, 2000; Kachadourian *et al.*, 2001; She *et al.*, 2007). 2-ME sensitized serum-starved fibroblasts to MG132-induced apoptosis but had little effect on MG132-treated proliferating fibroblasts (Figure 8D). This result is consistent with an important role for ROS homeostasis in serum-starved fibroblasts in ensuring cell viability in response to proteasome inhibition.

DISCUSSION

When a mammalian cell reversibly exits the cell cycle and enters quiescence, multiple mechanisms are evoked to protect the cell from differentiation, senescence, and apoptosis (Naderi *et al.*, 2003; Coller *et al.*, 2006; Sang *et al.*, 2008, 2010; Lemons *et al.*, 2010). In the present study, we demonstrated that proliferating and quiescent fibroblasts with the same genetic background respond differently to proteasome inhibition.

Whereas proliferating fibroblasts showed a dose-dependent increase in apoptotic cell death in response to proteasome inhibition, quiescent cells largely maintained viability (Figure 1). The resistance of quiescent cells to proteasome inhibition did not reflect a difference in proteasome-mediated degradation, because a comparable accumulation of ubiquitinated proteins and overall proteasome activity was observed in both proteasome-inhibited proliferating and quiescent fibroblasts (Figure 2). Instead, our findings suggest that quiescent fibroblasts employ multiple alternative protective mechanisms to avoid proteasome inhibition–mediated cell death. Such alternative mechanisms include autophagy/lysosomal–mediated degradation (Figure 3), reduced localization of ubiquitinated protein aggregates (Figure 5), and the detoxification of free radicals (Figure 8). It is intriguing that the extent to which quiescent fibroblasts used these alternative mechanisms depended on whether they were induced into quiescence by contact inhibition or serum starvation.

Proliferating and quiescent fibroblasts evoke a wide array of protective responses to proteasome inhibition, including the induction of cyclin-dependent kinase inhibitors, such as p27 and p21, that are expected to slow or pause the cell cycle and provide the cell with the time needed to clear accumulated proteins (Supplemental Figure S2D). Proteasome inhibition also resulted in the induction of chaperones that may aid in protein folding (Supplemental Figure S5). Our microarray analysis revealed that proteasome inhibition resulted in increased transcript levels of autophagy-related gene products (Figure 4 and Supplemental Table S1). We propose that this response reflects the cell's attempt to reduce proteasome activity by up-regulating an alternative, compensatory mechanism for clearing specific ubiquitinated proteins. Although the protective response to proteasome inhibition is engaged by both proliferating and quiescent fibroblasts, the phenotypic outcome is different in the different cell states.

Previous reports suggested that autophagy may play a compensatory role in protein clearance in cells with impaired proteasome activity (Pankiv *et al.*, 2007; Kirkin *et al.*, 2009; Korolchuk *et al.*,

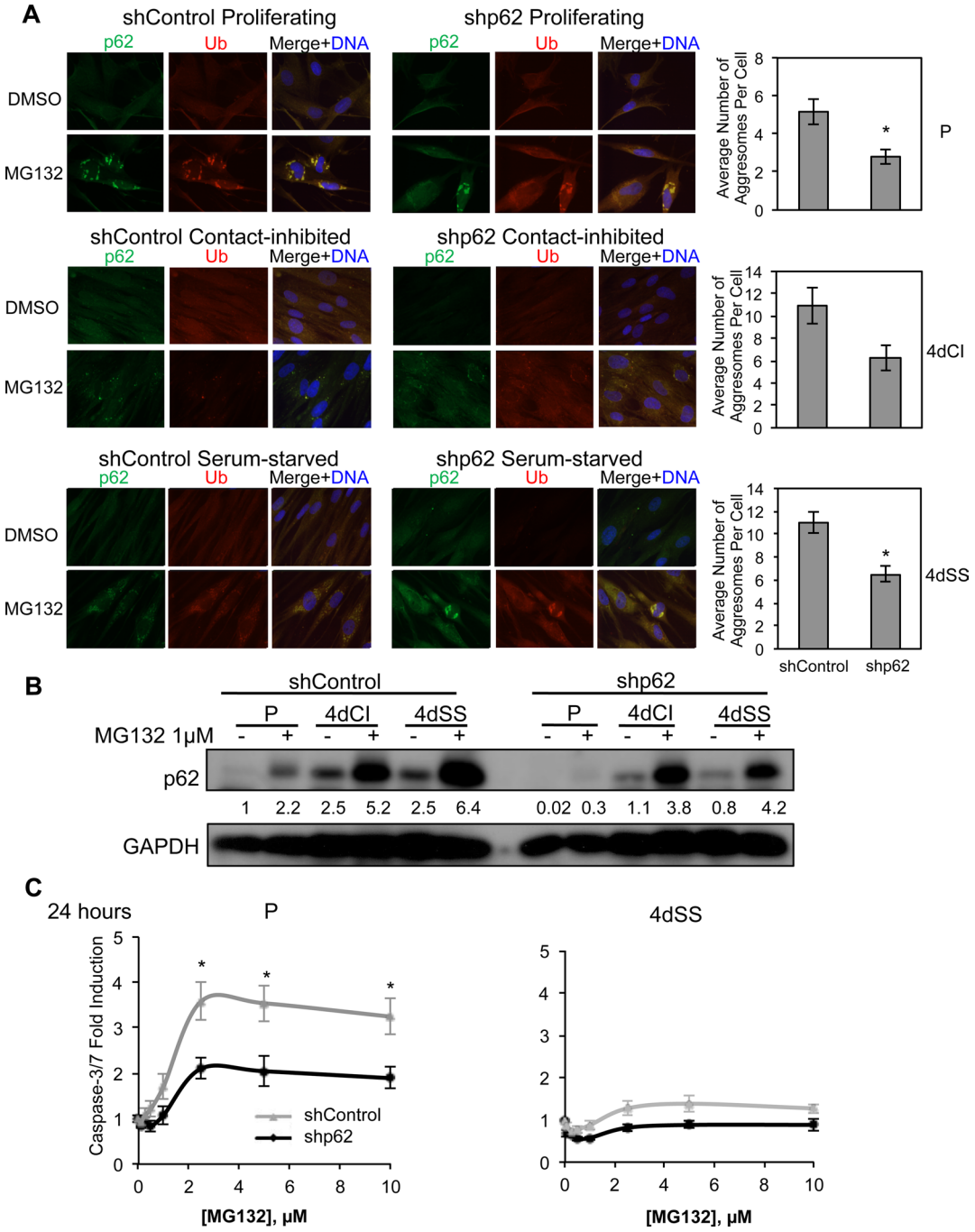

FIGURE 6: p62 knockdown results in reduced ubiquitinated protein aggregates and decreased apoptosis. (A) p62 knockdown results in fewer and smaller aggregates in response to proteasome inhibition. shp62- or nonsilencing shRNA control–expressing fibroblasts were plated on chamber slides under proliferating, contact-inhibited, and serum-starved conditions and treated with MG132 (1 μM) or DMSO for 24 h. Samples were fixed and stained with antibodies to p62 and ubiquitin. DNA was visualized by Hoechst staining. Images were taken at 40× magnification. Volocity software was used to quantify the number of aggresomes in images of MG132-treated proliferating and quiescent shControl- and shp62-expressing fibroblasts (five images each were used for shControl and shp62 proliferating and serum-starved cells and four images each were used for shControl and shp62 contact-inhibited fibroblasts). Area size cutoffs were 16–100 μm^2 for proliferating cells, 0.2–2 μm^2 for contact-inhibited cells, and 1–10 μm^2 for serum-starved cells. Asterisks indicate a statistically significant decrease in the number of aggresomes, $p < 0.05$. (B) An shRNA targeting p62 resulted in reduced p62 protein levels. Proliferating and quiescent fibroblasts expressing shp62 or shControl were treated with MG132 or DMSO for 24 h. p62 levels were monitored by immunoblot analysis. The ratio of p62 to GAPDH, normalized to DMSO (–) shControl, is reported. (C) p62 knockdown results in reduced apoptosis. Proliferating and serum-starved fibroblasts expressing shRNA to p62 or shControl were treated with increasing amounts of MG132 (0–10 μM) for 24 h. The experiments were performed three times in triplicate ($n = 9$). Apoptosis induction was monitored by caspase 3/7 activity assay, and the fold change compared with DMSO-treated control cells is shown. Asterisks indicate a statistically significant difference between p62 knockdown fibroblasts and shControl cells ($p < 0.05$).

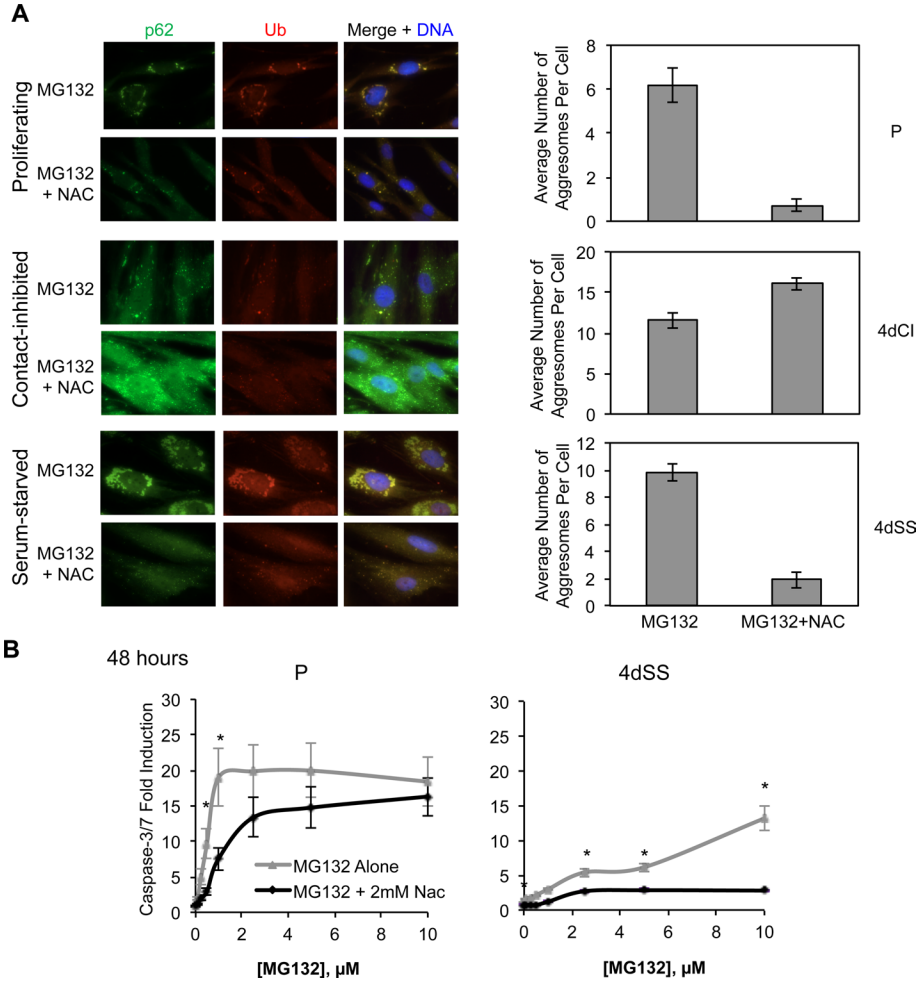

FIGURE 7: NAC protects fibroblasts from MG132-induced protein aggregation and apoptosis. (A) NAC treatment reduces intracellular, ubiquitin-positive aggregates for both proliferating and serum-starved, MG132-treated cells. Proliferating (P), contact-inhibited (4dCI), and serum-starved (4dSS) fibroblasts were treated with MG132 (1 μM) for 24 h in the presence or absence of NAC (2 mM). Samples were fixed and stained with antibodies to ubiquitin and p62. DNA was visualized by Hoechst staining. Images were taken at 40× magnification. Volocity software was used to quantify the number of aggresomes in ~10 images each of MG132 and MG132 plus NAC-treated proliferating, contact-inhibited, and serum-starved fibroblasts. Area size cutoffs were 16–100 μm^2 for proliferating cells, 0.2–2 μm^2 for contact-inhibited cells, and 1–10 μm^2 for serum-starved cells. (B) Proliferating and 4dSS fibroblasts were treated as in A for 48 h. For each sample, fold induction of caspase 3/7 activity relative to DMSO-treated cells is plotted. Data shown are averaged from three independent experiments, each performed in triplicate ($n = 9$). Error bars, SE. Asterisks indicate statistically significant differences between samples treated with MG132 and NAC compared with samples treated with MG132 alone ($p < 0.05$).

2009). Consistent with this observation, our results indicate a role for the autophagy/lysosomal degradation pathway in protecting serum-starved fibroblasts from proteasome inhibition–mediated apoptosis. First, autophagy was induced in quiescent fibroblasts and in response to MG132 treatment, which is consistent with previous reports (Valentin and Yang, 2008; Zhu *et al.*, 2010). Second, MG132- or bortezomib-induced apoptosis was potentiated by Baf treatment in serum-starved fibroblasts (Figure 3D and Supplemental Figure S3). By comparison, Baf treatment of proliferating fibroblasts resulted in a slight protection from MG132- or bortezomib-induced apoptosis (Figure 3D and Supplemental Figure S3) at 24 h posttreatment. Although synergy was not observed between the beclin-1 knockdown and MG132 treatment, beclin-1 knockdown sensitized proliferating fibroblasts to MG132-mediated apoptosis to a certain extent. Consistent with these observations, a myeloma cell line was recently reported to display a synergistic interaction between bortezomib and Baf even though atg5 knockdown did not synergize with bortezomib-induced cytotoxicity (Kawaguchi *et al.*, 2011). Our findings suggest that the Baf-sensitive autophagy/lysosomal pathways may be used to degrade aggregated ubiquitinated proteins and thereby decrease the load of ubiquitinated aggregates in serum-starved fibroblasts. Another possibility is that the sequestration of ubiquitinated proteins into autophagosomes in response to proteasome inhibition has a protective effect in proliferating cells, whereas the recycling of aggregated proteins in lysosomes is important for the viability of proteasome-inhibited, serum-starved cells. Moreover, Baf treatment also inhibits lysosome-mediated degradation, including mitophagy (Narendra *et al.*, 2008) and chaperone-mediated autophagy (Mizushima *et al.*, 2008). Accordingly, autophagy and/or other lysosomal pathways may also be implicated in the resistance of serum-starved fibroblasts to proteasome inhibition. Thus, our data strongly suggest that the Baf-sensitive autophagy/lysosomal pathways protect serum-starved fibroblasts from proteasome inhibition-mediated apoptosis.

Proteasome inhibition in proliferating fibroblasts resulted in the accumulation of juxtanuclear ubiquitin- and p62-positive aggregates, whereas ubiquitinated proteins were more dispersed in serum-starved fibroblasts and even more diffuse in contact-inhibited fibroblasts (Figure 5). Despite the induction of autophagy, proteasome-inhibited proliferating fibroblasts may not be as efficient at clearing aggregated proteins, thereby leading to an accumulation of aggregated proteins and increased toxicity. Alternatively, protein aggregation could directly contribute to apoptosis (Ling *et al.*, 2003; Fribley *et al.*, 2004; Perez-Galan *et al.*, 2006; Du *et al.*, 2009). For example, p62, a multifunctional protein reported to be involved in protein aggregation and the recruitment of ubiquitinated protein aggregates to autophagosomes for lysosomal degradation (Bjorkoy *et al.*, 2005; Pankiv *et al.*, 2007), has also been reported to induce the aggregation of caspase-8, which promotes its activation and triggers apoptosis (Jin *et al.*, 2009; Pan *et al.*, 2011). In primary fibroblasts, p62 knockdown reduced the levels of proteasome inhibition–mediated ubiquitinated protein aggregates and moderately reduced apoptosis at 24 h posttreatment (Figure 6). These findings are in accordance with a previous report indicating that p62 deletion decreases the accumulation of ubiquitin aggregates in the hepatocytes of autophagy-deficient mice (Komatsu *et al.*, 2007). Thus, in this instance, a reduction in p62 levels may affect both the accumulation of ubiquitinated aggregates and apoptosis through the same or distinct mechanisms. Our data suggest a correlation between

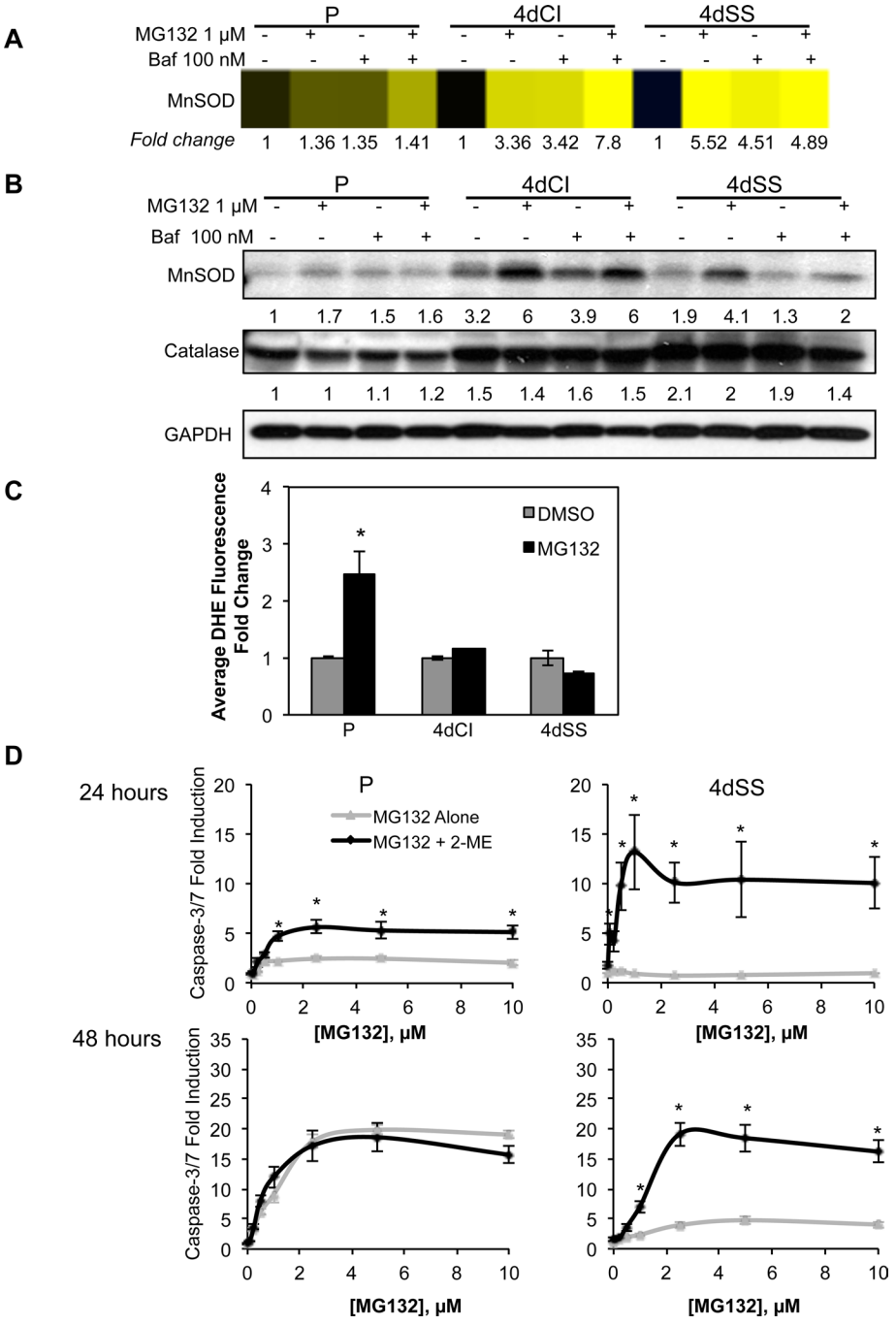

FIGURE 8: MG132 treatment increases cellular superoxide levels in proliferating but not quiescent fibroblasts, and 2-ME sensitizes serum-starved quiescent fibroblasts to proteasome inhibition. (A, B) MG132 treatment resulted in up-regulation of MnSOD at transcript and protein levels. (A) MnSOD expression was determined by microarray as in Figure 4. Heat map displaying the results and fold change of each treated sample, normalized to DMSO-treated control, is shown. Yellow indicates increased expression compared with the DMSO control for cells in the indicated proliferative state. (B) MnSOD and catalase are expressed at higher levels in quiescent than in proliferating fibroblasts. Cells were treated as indicated for 24 h, and protein expression was monitored by immunoblot analysis. GADPH was used as a loading control. For each protein, the ratio of protein intensity to GAPDH intensity, normalized to proliferating DMSO (–) control, is shown. (C) Total cellular superoxide levels are increased in MG132-treated proliferating but not contact-inhibited or serum-starved fibroblasts. Cells in different proliferative conditions were treated with DMSO or MG132 and monitored for superoxide levels by incubating with the dye DHE, followed by flow cytometry. Average fold change normalized to proliferating DMSO control is shown from two experiments, each performed in duplicate ($n = 4$). Error bars, SE; the asterisk indicates a statistically significant difference between proliferating MG132 and DMSO-treated cells ($p < 0.05$). (D) Proliferating and 4dSS fibroblasts were treated with increasing doses of MG132 (0–10 μM) for the indicated times in the presence or absence of 100 μM 2-ME, which was introduced for the last 6 h of MG132 treatment. Fold induction of caspase 3/7 activity is plotted. The average of three independent experiments, each performed in triplicate ($n = 9$), is shown. Error bars indicate standard errors. Asterisks indicate statistically significant differences between samples treated with MG132 plus 2-ME vs. MG132 alone at each dosage ($p < 0.05$).

intracellular ubiquitinated protein aggregation and apoptosis in response to proteasome inhibition. Accordingly, limited protein aggregation may have a cytoprotective effect, but a more extensive accumulation of protein aggregates is ultimately cytotoxic. Thus, in quiescent fibroblasts, mechanisms that reduce the accumulation of ubiquitinated protein aggregates may protect the cell from proteasome inhibition–mediated apoptosis and cell death.

Our data also strongly support a role for free radicals in proteasome inhibition–mediated protein aggregation and apoptosis. In several cell lines, high ROS levels caused by proteasome inhibition induce protein aggregation and apoptotic cell death (Ling *et al.*, 2003; Fribley *et al.*, 2004; Perez-Galan *et al.*, 2006; Du *et al.*, 2009). For example, treatment of fibroblasts with the antioxidant NAC reduced the extent of MG132-induced apoptosis and ubiquitinated protein aggregates, especially in proliferating and serum-starved fibroblasts (Figure 7). The elevated levels of ROS-detoxifying enzymes in quiescent cells (Figure 8B) may protect them from proteasome inhibition–mediated cell death, as levels of the ROS-detoxifying enzymes MnSOD and catalase are higher in quiescent fibroblasts than proliferating fibroblasts (Figure 8B). Proteasome-inhibited quiescent fibroblasts have higher levels of MnSOD than do proteasome-inhibited proliferating fibroblasts, which would be expected to reduce the levels of mitochondrially derived ROS, a potential cause of damage to cellular components. Consistent with this effect, proliferating fibroblasts exhibit increased superoxide levels in response to proteasome inhibition, whereas in serum-starved fibroblasts, superoxide levels did not increase. Furthermore, we found that increasing intracellular superoxide concentrations with 2-ME sensitized serum-starved quiescent fibroblasts to MG132-induced apoptosis (Figure 8D). Restricting the accumulation of mitochondrially derived superoxide anions via MnSOD may be important for maintaining quiescent fibroblasts in a nondividing

state because decreases in MnSOD in quiescent mouse embryonic fibroblasts have been reported to cause cell cycle reentry (Sarsour *et al.*, 2008). Thus our data indicate that ROS-detoxifying pathways engaged during quiescence may also play a central role in the protection against proteasome inhibition.

In summary, our research indicates that in quiescent primary fibroblasts, Baf-sensitive autophagy/lysosomal pathways, ROS-detoxifying enzymes, and mechanisms that reduce protein aggregation may individually or collectively protect cells from proteasome inhibition–mediated apoptosis and cell death. Our findings further suggest that the precise mechanism(s) through which quiescent cells survive proteasome inhibition vary depending on the quiescence-inducing signal, that is, contact inhibition versus serum starvation. Further investigation into these compensatory protective mechanisms will elucidate the mechanism by which quiescent cells resist proteasome inhibition–mediated cell death via the orchestration of a complex network of protective mechanisms and alternative pathways. Deciphering the protective mechanisms evoked upon quiescence may ultimately contribute to improving the effectiveness of proteasome inhibitors in cancer treatment.

MATERIALS AND METHODS

Cell culture

Human primary foreskin fibroblasts were isolated as previously described (Legesse-Miller *et al.*, 2009). Fibroblasts were maintained in DMEM (Invitrogen-GIBCO, Carlsbad, CA) supplemented with 10% fetal bovine serum (FBS; Atlanta Biologicals, Lawrenceville, GA) and 100 μg/ml penicillin and streptomycin (Invitrogen, Carlsbad, CA) or in fibroblast basal medium supplemented with 2% fetal bovine serum, fibroblast growth factor, insulin, and gentamicin (Lonza, Basel, Switzerland).

Antibodies and reagents

Anti-LC3, anti–beclin-1, anti-ubiquitin (P4D1), and anti-HSP70 antibodies, and HSP/chaperone antibody sample kit were purchased from Cell Signaling (Danvers, MA). Anti-p27, anti-SUG1, anti-PSMB1, anti-PSMB2, anti-PSMB5, and anti-ubiquitin antibodies were purchased from Santa Cruz Biotechnology (Santa Cruz, CA). Anti-GAPDH antibody was purchased from Abcam (Cambridge, MA). Anti-p21 antibody was purchased from BD Biosciences (San Jose, CA). Anti-p62 antibody and Baf were purchased from Enzo Life Sciences (Farmingdale, NY). PI was purchased from VWR (West Chester, PA). RNase A was purchased from Thermo Fisher Scientific (Waltham, MA). DMSO was purchased from the American Type Culture Collection (Manassas, VA). Carbobenzoxy-Leu-Leu-leucinal (MG132) and epoxomicin were purchased from Calbiochem (Gibbstown, NJ). Bortezomib was purchased from LC Laboratories (Woburn, MA). Annexin V conjugated to Alexa Fluor 350 was purchased from Invitrogen. NAC and 2-ME were purchased from Sigma-Aldrich (St. Louis, MO).

Proteasome and autophagy inhibition

For proliferating cells, 4×10^5 cells per 10-cm dish were seeded in DMEM containing 10% FBS. Twenty-four hours postseeding, MG132, epoxomicin, lactacystin, Baf (all dissolved in DMSO), or an equal volume of DMSO was added directly to the medium. To induce quiescence through contact inhibition, cells were grown in DMEM containing 10% FBS medium for 4 d and then treated with a proteasome inhibitor or vehicle control. To induce quiescence through serum starvation, the medium was changed to serum starvation medium (DMEM containing 0.1% FBS) 24 h postseeding and the cells were incubated for 4 d and then treated with a proteasome inhibitor or DMSO control. In all cases, medium was changed 24 h before proteasome treatment. Except where otherwise indicated, MG132 was used at 1 μM and Baf was used at 100 nM.

PI exclusion assay for live/dead analysis

Cell viability analysis with PI exclusion assay was performed as described previously (Lemons *et al.*, 2010). Proliferating and quiescent (contact-inhibited or serum-starved) cells were treated with the indicated drugs or DMSO control and then collected, centrifuged, and resuspended with phosphate-buffered saline (PBS) containing 5% FBS and 0.5 mg/ml PI. The cells were immediately analyzed by flow cytometry using a BD LSRII multilaser analyzer (BD Biosciences). At least 20,000 cells were analyzed with FACSDiVa software (BD Biosciences). PI-negative cells were counted as live cells, and PI-positive cells were counted as dead cells. For each proliferative condition, the fraction of cells that were viable in the DMSO-treated sample was adjusted to 100%, and other treatments were expressed in relation to the DMSO sample.

Apoptosis analysis with annexin V staining

Proliferating, contact-inhibited, and serum-starved cells were treated with MG132 or vehicle control (DMSO) for 24 or 48 h. The cells were trypsinized and collected into their own conditioned medium and centrifuged for 5 min at 1000 rpm. The cells were washed with PBS and resuspended at ~1×10^6 cells/0.5 ml of annexin-binding buffer (10 mM 4-(2-hydroxyethyl)-1-piperazineethanesulfonic acid, pH 7.4, 140 mM NaCl, and 2.5 mM $CaCl_2$). In total, 5 μl of annexin V conjugate and 0.5 μl of 1 mg/ml PI were added to each 100-μl aliquot of cell suspension. After a 15-min incubation at room temperature, 400 μl of annexin-binding buffer was added, and the cells were analyzed using the BD LSRII flow cytometer. At least 10,000 cells were collected and analyzed with FACSDiVa software. Dead cells were indicated with PI, which was detected with excitation and emission at 560 and 595 nm, respectively. Apoptotic cells were stained with annexin V conjugated to Alexa Fluor 350 and were detected with excitation and emission at 346 and 442 nm, respectively.

Intracellular superoxide levels measurement

To monitor intracellular superoxide levels, we incubated cells with DHE in DMEM at a concentration of 1 μM per 150,000 cells in 0.5× Serum Replacement 3 solution (Sigma-Aldrich) for 30 min at 37°C and 5% CO_2. Cells in the same proliferative state were collected unstained. The cells were analyzed by flow cytometry using a BD LSRII multilaser analyzer with FACSDiVa software. The cells were excited at 488 nm, and emission was collected using a 575/26 nm filter. A total of 1×10^4 live cells was recorded. The cells were gated on forward/side scatter plots. The intensity of staining in stained minus unstained cells was reported.

Cell cycle analysis

Cell cycle analysis was performed as described previously (Lemons *et al.*, 2010). Untreated and treated (DMSO or MG132) proliferating and quiescent (contact-inhibited or serum-starved) cells were trypsinized and fixed with 67% ethanol in PBS at 4°C. The cells were centrifuged and washed with PBS. The cell pellets were resuspended with PBS containing PI (40 μg/ml) and RNase A (200 μg/ml) and incubated for 1 h at room temperature. PI fluorescence was monitored with BD LSRII multilaser analyzer flow cytometry using FACSDiVa software. Cell cycle distributions were determined with ModFit LT software using the Watson Pragmatics algorithm.

Apoptosis analysis with luminescent substrates

Apoptosis was determined using the ApoLive-Glo Assay Kit (Promega, Madison, WI) according to the manufacturer's instructions. Cells were plated in triplicate at 5000 or 10,000 cells/well in white-walled, clear-bottomed 96-well plates (Costar, Lowell, MA). For serum starvation, the cells were plated 4 d before treatment in serum starvation medium (0.1% FBS). Proliferating cells were plated 24 h before the start of treatment. Increasing concentrations of MG132 or bortezomib alone or together with Baf (100 nM), NAC (2 mM), or 2-ME (100 µM) were added to each well, and the cells were incubated for 24, 48, or 72 h. At the indicated times, 100 µl of the apoptosis reagent (ApoLive Glo Assay Kit; Promega) was added. Plates were incubated for 1 h at room temperature. Luminescence (caspase 3/7 activity) was read from the top using the Synergy MX plate reader (Biotek Instruments, Winooski, VT).

Immunoblot analysis

The cells were lysed in RIPA buffer containing protease and phosphatase inhibitors (10 mM $NaPO_4$, pH 7.2, 0.3 M NaCl, 0.1% SDS, 1% NP40, 1% Na deoxycholate, 2 mM EDTA, protease inhibitor cocktail [Roche, Nutley, N], and Halt Phosphatase Inhibitor [Thermo Fisher Scientific, Pittsburgh, PA]). Protein concentrations were determined using the Bio-Rad protein assay (Bio-Rad, Hercules, CA). Equal amounts of total cellular proteins were resolved on SDS–PAGE and electrotransferred onto a polyvinylidene fluoride membrane, which was then incubated with the indicated antibodies. Secondary antibodies were conjugated with horseradish peroxidase, and enhanced chemiluminescence (Amersham Pharmacia, Piscataway, NJ) was used to detect the antigen. The membranes were stripped using Restore Western Blot Stripping Buffer (Thermo Scientific) and reacted with GAPDH. GAPDH was used as a loading control.

Viral infection and knockdown cell preparation

Beclin-1 shRNA in the LMP retroviral shRNA vector and an empty vector control were a gift of Eileen White (Cancer Institute of New Jersey, Rutgers University). Lentiviral vectors pLKO.1 containing a nonsense shRNA sequence (shControl) or shp62 were purchased from Sigma-Aldrich. Transfections were performed with Arrest-In transfection reagent (Open Biosystems, Huntsville, AL) diluted in Opti-MEM reduced serum medium (Invitrogen). For retroviral transduction, 5 µg of viral construct DNA and 5 µg of AmphoHelper packaging DNA (Orbigen, San Diego, CA) were cotransfected into Phoenix cells (Orbigen) with 5 µg/ml polybrene. For lentiviral transduction, construct DNA (4.1 µg) and 2 µg each of Δ8.9 and vesicular stomatitis virus G packaging vectors were cotransfected into HEK293FT cells (Open Biosystems). Viral supernatant was filtered and incubated with low-passage fibroblasts for 48 h. Virally infected fibroblasts were selected with 2 µg/ml puromycin (Invitrogen).

Indirect immunofluorescence

Cells were grown in Millicell EZ chamber slides (Millipore, Billerica, MA) and treated with reagents as indicated for 24 h. Cells were fixed with 4% formaldehyde, permeabilized with ice-cold methanol at –20°C, blocked with PBS containing 5% bovine serum albumin and 0.2% Triton X-100, and stained with primary antibodies as indicated, followed by Alexa Flour 488– and Alexa Flour 633–conjugated fluorescent secondary antibodies (Invitrogen) for visualization. The samples were stained with Hoechst to visualize DNA. The cells were washed with PBS and mounted with a drop of Antifade Prolong Solution (Invitrogen). Images were acquired using an Olympus IX81 inverted fluorescence microscope (Olympus, Melville, NY) with a filter cube containing UV light and 488- and 633-nm filters. Volocity software (PerkinElmer, Waltham, MA) was used for image acquisition and analysis.

Microarray analysis

Proliferating, contact-inhibited, and serum-starved fibroblasts were treated with DMSO, 1 µM MG132, 100 nM Baf, or 1 µM MG132 and 100 nM Baf for 24 h. Total RNA was isolated using the MirVana miRNA isolation kit (Ambion, Austin, TX). RNA quality was verified using a Bioanalyzer 2100 (Agilent Technology, Santa Clara, CA), and the amount was determined with a NanoDrop spectrophotometer (NanoDrop Technologies, Wilmington, DE). Total RNA (500 ng) was amplified using the Low RNA Input Fluorescent Labeling Kit (Agilent Technologies). Cyanine 3-CTP (Cy-3) (PerkinElmer) was directly incorporated into the cRNA from DMSO-treated cells for each cell state during in vitro transcription. Cyanine 5-CTP (Cy-5) was incorporated into cRNA from DMSO, MG132, Baf, and MG132 and Baf-treated fibroblasts. Mixtures of Cy-3 and Cy-5 labeled cRNA were cohybridized to Whole Human Genome Oligo Microarray slides (Agilent Technologies) at 60°C for 17 h and subsequently washed according to the Agilent hybridization protocol. Slides were scanned with a dual-laser scanner (Agilent Technologies). The Agilent feature extraction software, in conjunction with the Princeton University Microarray database (PUMAdb; http://puma.princeton.edu), was used to compute the log ratio of the two samples for each gene after background subtraction and dye normalization. Of the 44,000 probes on the microarray, 21,467 probes generated signal in 10 of 12 arrays. The probes from these data were mapped to genes based on UniGene Clusters. If multiple probes mapped to a single gene, the values were averaged. Genes for which the absolute value among the microarrays varied by more than twofold were selected for analysis, resulting in 6879 genes. These genes were clustered with the *K*-means algorithm using Cluster software (de Hoon *et al.*, 2004) into 10 groups. The clustered data were visualized by Java TreeView (de Hoon *et al.*, 2004) in heat map format. The Lewis–Sigler Institute for Integrative Genomics portal to GO Term Finder was used to determine the probability of observing a statistically significant number of genes with a specific Gene Ontology classification in a *K*-means cluster (http://go.princeton.edu/cgibin/GOTermFinder/GOTermFinder).

Filter trap assay

Proliferating, contact-inhibited, and serum-starved cells were treated for 24 h with MG132 or DMSO. Cells were lysed with buffer containing 20 mM Tris, pH 7.5, 137 mM NaCl, and protease and phosphatase inhibitor cocktails and sonicated for 1 min. Protein concentrations were determined using bicinchoninic acid (Pierce Biotechnology, Rockford, IL). A 30-µg amount of protein was mixed with SDS at a final concentration of 1%, and the samples were boiled for 10 min at 95°C. The samples were then loaded onto a slot blot apparatus (Hybri-Slot Manifold, Life Technologies-BRL, San Francisco, CA) and filtered through a 0.2 µM cellulose acetate membrane (Bethesda Research Laboratories, Grand Island, NY). Aggregated proteins were detected by probing the membrane with anti-ubiquitin antibodies.

Aggresome size and number measurements

Aggresomes were quantified using Volocity 6.1.1 3D Image Analysis software. To quantify aggresome size, the line tool was used to measure the longest length. Calculations of the number of aggresomes were made using an area size cutoff of 16–100 μm^2 for proliferating cells, 0.2–2 μm^2 for contact-inhibited cells, and 1–10 μm^2 for serum-starved cells. For proliferating and serum-starved states, ~60 cells were quantified in each condition. Approximately 100 cells were

quantified for the contact-inhibited state. Images from two independent experiments were quantified in each figure.

Statistical analysis

Statistical significance was determined by two-sample, unpaired two-tailed Student's *t* tests, assuming equal variances.

ACKNOWLEDGMENTS

We thank the following individuals, all at Princeton University except as indicated: Lee Fischer, Robert Alex Stokes, Daniel Wolle, Amanda Joy Guise, Matthew Remillard, Mina Kojima, Jessica Buckles, Donna Storton, John Matese, and Christina DeCoste for experimental assistance, Eileen White (Cancer Institute of New Jersey, Rutgers University) for the beclin-1 retroviral constructs, and Jane Flint, Jeffry Stock, and Leonid Kruglyak, as well as the entire Coller lab, for helpful and insightful discussions. This work was supported by National Cancer Institute Grant K01 CA128887 to A.L.-M and by National Institute of General Medical Sciences Center of Excellence Grant P50 GM071508, the Rita Allen Foundation, the Cancer Institute of New Jersey, the New Jersey Commission on Cancer Research, National Cancer Institute Grant 1RC1 CA147961-01, a Focused Funding Grant to H.A.C. from the Johnson & Johnson Foundation, and a grant from the PhRMA Foundation to H.A.C. (2007RSGl9572).

REFERENCES

Bjorkoy G, Lamark T, Brech A, Outzen H, Perander M, Overvatn A, Stenmark H, Johansen T (2005). p62/SQSTM1 forms protein aggregates degraded by autophagy and has a protective effect on huntingtin-induced cell death. J Cell Biol 171, 603–614.

Bjorkoy G, Lamark T, Johansen T (2006). p62/SQSTM1: a missing link between protein aggregates and the autophagy machinery. Autophagy 2, 138–139.

Brandeis M, Hunt T (1996). The proteolysis of mitotic cyclins in mammalian cells persists from the end of mitosis until the onset of S phase. EMBO J 15, 5280–5289.

Bush KT, Goldberg AL, Nigam SK (1997). Proteasome inhibition leads to a heat-shock response, induction of endoplasmic reticulum chaperones, and thermotolerance. J Biol Chem 272, 9086–9092.

Cao Y, Klionsky DJ (2007). Physiological functions of Atg6/beclin 1: a unique autophagy-related protein. Cell Res 17, 839–849.

Chauhan D, Hideshima T, Mitsiades C, Richardson P, Anderson KC (2005). Proteasome inhibitor therapy in multiple myeloma. Mol Cancer Ther 4, 686–692.

Ciechanover A (2005). Proteolysis: from the lysosome to ubiquitin and the proteasome. Nat Rev Mol Cell Biol 6, 79–87.

Coller HA, Sang L, Roberts JM (2006). A new description of cellular quiescence. PLoS Biol 4, e83.

Cuervo AM (2004). Autophagy: in sickness and in health. Trends Cell Biol 14, 70–77.

de Hoon MJ, Imoto S, Nolan J, Miyano S (2004). Open source clustering software. Bioinformatics 20, 1453–1454.

Ding WX, Ni HM, Gao W, Yoshimori T, Stolz DB, Ron D, Yin XM (2007). Linking of autophagy to ubiquitin-proteasome system is important for the regulation of endoplasmic reticulum stress and cell viability. Am J Pathol 171, 513–524.

Dreger H, Westphal K, Wilck N, Baumann G, Stangl V, Stangl K, Meiners S (2010). Protection of vascular cells from oxidative stress by proteasome inhibition depends on Nrf2. Cardiovasc Res 85, 395–403.

Drexler HC, Risau W, Konerding MA (2000). Inhibition of proteasome function induces programmed cell death in proliferating endothelial cells. FASEB J 14, 65–77.

Du ZX, Zhang HY, Meng X, Guan Y, Wang HQ (2009). Role of oxidative stress and intracellular glutathione in the sensitivity to apoptosis induced by proteasome inhibitor in thyroid cancer cells. BMC Cancer 9, 56.

Dulic V, Stein GH, Far DF, Reed SI (1998). Nuclear accumulation of $p21^{Cip1}$ at the onset of mitosis: a role at the G2/M-phase transition. Mol Cell Biol 18, 546–557.

Fribley A, Zeng Q, Wang CY (2004). Proteasome inhibitor PS-341 induces apoptosis through induction of endoplasmic reticulum stress-reactive oxygen species in head and neck squamous cell carcinoma cells. Mol Cell Biol 24, 9695–9704.

Goldberg AL (2003). Protein degradation and protection against misfolded or damaged proteins. Nature 426, 895–899.

Gordon C, McGurk G, Wallace M, Hastie ND (1996). A conditional lethal mutant in the fission yeast 26 S protease subunit mts3+ is defective in metaphase to anaphase transition. J Biol Chem 271, 5704–5711.

Goy A *et al.* (2005). Phase II study of proteasome inhibitor bortezomib in relapsed or refractory B-cell non-Hodgkin's lymphoma. J Clin Oncol 23, 667–675.

Han YH, Kim SZ, Kim SH, Park WH (2010). Reactive oxygen species and glutathione level changes by a proteasome inhibitor, MG132, partially affect calf pulmonary arterial endothelial cell death. Drug Chem Toxicol 33, 403–409.

Han YH, Park WH (2010). The changes of reactive oxygen species and glutathione by MG132, a proteasome inhibitor affect As4.1 juxtaglomerular cell growth and death. Chem Biol Interact 184, 319–327.

Heinemeyer W, Fischer M, Krimmer T, Stachon U, Wolf DH (1997). The active sites of the eukaryotic 20 S proteasome and their involvement in subunit precursor processing. J Biol Chem 272, 25200–25209.

Hideshima T, Richardson P, Chauhan D, Palombella VJ, Elliott PJ, Adams J, Anderson KC (2001). The proteasome inhibitor PS-341 inhibits growth, induces apoptosis, and overcomes drug resistance in human multiple myeloma cells. Cancer Res 61, 3071–3076.

Huang P, Feng L, Oldham EA, Keating MJ, Plunkett W (2000). Superoxide dismutase as a target for the selective killing of cancer cells. Nature 407, 390–395.

Huo LJ, Zhong ZS, Liang CG, Wang Q, Yin S, Ai JS, Yu LZ, Chen DY, Schatten H, Sun QY (2006). Degradation of securin in mouse and pig oocytes is dependent on ubiquitin-proteasome pathway and is required for proteolysis of the cohesion subunit, Rec8, at the metaphase-to-anaphase transition. Front Biosci 11, 2193–2202.

Iwata J, Ezaki J, Komatsu M, Yokota S, Ueno T, Tanida I, Chiba T, Tanaka K, Kominami E (2006). Excess peroxisomes are degraded by autophagic machinery in mammals. J Biol Chem 281, 4035–4041.

Janen SB, Chaachouay H, Richter-Landsberg C (2010). Autophagy is activated by proteasomal inhibition and involved in aggresome clearance in cultured astrocytes. Glia 58, 1766–1774.

Jin Z, Li Y, Pitti R, Lawrence D, Pham VC, Lill JR, Ashkenazi A (2009). Cullin3-based polyubiquitination and p62-dependent aggregation of caspase-8 mediate extrinsic apoptosis signaling. Cell 137, 721–735.

Jung T, Catalgol B, Grune T (2009). The proteasomal system. Mol Aspects Med 30, 191–296.

Kachadourian R, Liochev SI, Cabelli DE, Patel MN, Fridovich I, Day BJ (2001). 2-Methoxyestradiol does not inhibit superoxide dismutase. Arch Biochem Biophys 392, 349–353.

Kawaguchi T, Miyazawa K, Moriya S, Ohtomo T, Che XF, Naito M, Itoh M, Tomoda A (2011). Combined treatment with bortezomib plus bafilomycin A1 enhances the cytocidal effect and induces endoplasmic reticulum stress in U266 myeloma cells: crosstalk among proteasome, autophagy-lysosome and ER stress. Int J Oncol 38, 643–654.

Kegel KB, Kim M, Sapp E, McIntyre C, Castano JG, Aronin N, DiFiglia M (2000). Huntingtin expression stimulates endosomal-lysosomal activity, endosome tubulation, and autophagy. J Neurosci 20, 7268–7278.

Kirkin V *et al.* (2009). A role for NBR1 in autophagosomal degradation of ubiquitinated substrates. Mol Cell 33, 505–516.

Klionsky *et al.* (2008). Guidelines for the use and interpretation of assays for monitoring autophagy in higher eukaryotes. Autophagy 4, 151–175.

Klionsky DJ (2005). The molecular machinery of autophagy: unanswered questions. J Cell Sci 118, 7–18.

Komatsu M *et al.* (2006). Loss of autophagy in the central nervous system causes neurodegeneration in mice. Nature 441, 880–884.

Komatsu M *et al.* (2007). Homeostatic levels of p62 control cytoplasmic inclusion body formation in autophagy-deficient mice. Cell 131, 1149–1163.

Komatsu M *et al.* (2005). Impairment of starvation-induced and constitutive autophagy in Atg7-deficient mice. J Cell Biol 169, 425–434.

Korolchuk VI, Mansilla A, Menzies FM, Rubinsztein DC (2009). Autophagy inhibition compromises degradation of ubiquitin-proteasome pathway substrates. Mol Cell 33, 517–527.

Kuma A, Hatano M, Matsui M, Yamamoto A, Nakaya H, Yoshimori T, Ohsumi Y, Tokuhisa T, Mizushima N (2004). The role of autophagy during the early neonatal starvation period. Nature 432, 1032–1036.

Lee AH, Iwakoshi NN, Anderson KC, Glimcher LH (2003). Proteasome inhibitors disrupt the unfolded protein response in myeloma cells. Proc Natl Acad Sci USA 100, 9946–9951.

Lee DH, Goldberg AL (1998). Proteasome inhibitors: valuable new tools for cell biologists. Trends Cell Biol 8, 397–403.
Legesse-Miller A, Elemento O, Pfau SJ, Forman JJ, Tavazoie S, Coller HA (2009). let-7 overexpression leads to an increased fraction of cells in G2/M, direct down-regulation of Cdc34, and stabilization of Wee1 kinase in primary fibroblasts. J Biol Chem 284, 6605–6609.
Lemons JM, Feng XJ, Bennett BD, Legesse-Miller A, Johnson EL, Raitman I, Pollina EA, Rabitz HA, Rabinowitz JD, Coller HA (2010). Quiescent fibroblasts exhibit high metabolic activity. PLoS Biol 8, e1000514.
Ling YH, Liebes L, Zou Y, Perez-Soler R (2003). Reactive oxygen species generation and mitochondrial dysfunction in the apoptotic response to bortezomib, a novel proteasome inhibitor, in human H460 non-small cell lung cancer cells. J Biol Chem 278, 33714–33723.
Maattanen P, Gehring K, Bergeron JJ, Thomas DY (2010). Protein quality control in the ER: the recognition of misfolded proteins. Semin Cell Dev Biol 21, 500–511.
Maher P (2008). Proteasome inhibitors prevent oxidative stress-induced nerve cell death by a novel mechanism. Biochem Pharmacol 75, 1994–2006.
Marambio P *et al*. (2010). Glucose deprivation causes oxidative stress and stimulates aggresome formation and autophagy in cultured cardiac myocytes. Biochim Biophys Acta 1802, 509–518.
Mathew A, Morimoto RI (1998). Role of the heat-shock response in the life and death of proteins. Ann NY Acad Sci 851, 99–111.
Mathew R, Kongara S, Beaudoin B, Karp CM, Bray K, Degenhardt K, Chen G, Jin S, White E (2007). Autophagy suppresses tumor progression by limiting chromosomal instability. Genes Dev 21, 1367–1381.
Milani M, Rzymski T, Mellor HR, Pike L, Bottini A, Generali D, Harris AL (2009). The role of ATF4 stabilization and autophagy in resistance of breast cancer cells treated with Bortezomib. Cancer Res 69, 4415–4423.
Mizushima N, Levine B, Cuervo AM, Klionsky DJ (2008). Autophagy fights disease through cellular self-digestion. Nature 451, 1069–1075.
Naderi J, Hung M, Pandey S (2003). Oxidative stress-induced apoptosis in dividing fibroblasts involves activation of p38 MAP kinase and over-expression of Bax: resistance of quiescent cells to oxidative stress. Apoptosis 8, 91–100.
Narendra D, Tanaka A, Suen DF, Youle RJ (2008). Parkin is recruited selectively to impaired mitochondria and promotes their autophagy. J Cell Biol 183, 795–803.
Pan JA, Ullman E, Dou Z, Zong WX (2011). Inhibition of protein degradation induces apoptosis through a microtubule-associated protein 1 light chain 3-mediated activation of caspase-8 at intracellular membranes. Mol Cell Biol 31, 3158–3170.
Pankiv S, Clausen TH, Lamark T, Brech A, Bruun JA, Outzen H, Overvatn A, Bjorkoy G, Johansen T (2007). p62/SQSTM1 binds directly to Atg8/LC3 to facilitate degradation of ubiquitinated protein aggregates by autophagy. J Biol Chem 282, 24131–24145.
Perez-Galan P, Roue G, Villamor N, Montserrat E, Campo E, Colomer D (2006). The proteasome inhibitor bortezomib induces apoptosis in mantle-cell lymphoma through generation of ROS and Noxa activation independent of p53 status. Blood 107, 257–264.
Ravikumar B, Duden R, Rubinsztein DC (2002). Aggregate-prone proteins with polyglutamine and polyalanine expansions are degraded by autophagy. Hum Mol Genet 11, 1107–1117.
Ravikumar B *et al*. (2004). Inhibition of mTOR induces autophagy and reduces toxicity of polyglutamine expansions in fly and mouse models of Huntington disease. Nat Genet 36, 585–595.
Reed SI (2006). The ubiquitin-proteasome pathway in cell cycle control. Results Probl Cell Differ 42, 147–181.
Sang L, Coller HA (2009). Fear of commitment: Hes1 protects quiescent fibroblasts from irreversible cellular fates. Cell Cycle 8, 2161–2167.
Sang L, Coller HA, Roberts JM (2008). Control of the reversibility of cellular quiescence by the transcriptional repressor HES1. Science 321, 1095–1100.
Sang L, Roberts JM, Coller HA (2010). Hijacking HES1: how tumors co-opt the anti-differentiation strategies of quiescent cells. Trends Mol Med 16, 17–26.
Sarsour EH, Venkataraman S, Kalen AL, Oberley LW, Goswami PC (2008). Manganese superoxide dismutase activity regulates transitions between quiescent and proliferative growth. Aging Cell 7, 405–417.
Schewe DM, Aguirre-Ghiso JA (2008). ATF6alpha-Rheb-mTOR signaling promotes survival of dormant tumor cells in vivo. Proc Natl Acad Sci USA 105, 10519–10524.
Schewe DM, Aguirre-Ghiso JA (2009). Inhibition of eIF2alpha dephosphorylation maximizes bortezomib efficiency and eliminates quiescent multiple myeloma cells surviving proteasome inhibitor therapy. Cancer Res 69, 1545–1552.
She MR, Li JG, Guo KY, Lin W, Du X, Niu XQ (2007). Requirement of reactive oxygen species generation in apoptosis of leukemia cells induced by 2-methoxyestradiol. Acta Pharmacol Sin 28, 1037–1044.
Sherman MY, Goldberg AL (2001). Cellular defenses against unfolded proteins: a cell biologist thinks about neurodegenerative diseases. Neuron 29, 15–32.
Skaar JR, Pagano M (2009). Control of cell growth by the SCF and APC/C ubiquitin ligases. Curr Opin Cell Biol 21, 816–824.
Takeda K, Yanagida M (2010). In quiescence of fission yeast, autophagy and the proteasome collaborate for mitochondrial maintenance and longevity. Autophagy 6, 564–565.
Takeda K, Yoshida T, Kikuchi S, Nagao K, Kokubu A, Pluskal T, Villar-Briones A, Nakamura T, Yanagida M (2010). Synergistic roles of the proteasome and autophagy for mitochondrial maintenance and chronological lifespan in fission yeast. Proc Natl Acad Sci USA 107, 3540–3545.
Tamura D *et al*. (2010). Bortezomib potentially inhibits cellular growth of vascular endothelial cells through suppression of G2/M transition. Cancer Sci 101, 1403–1408.
Tsukada M, Ohsumi Y (1993). Isolation and characterization of autophagy-defective mutants of *Saccharomyces cerevisiae*. FEBS Lett 333, 169–174.
Vadlamudi RK, Joung I, Strominger JL, Shin J (1996). p62, a phosphotyrosine-independent ligand of the SH2 domain of p56lck, belongs to a new class of ubiquitin-binding proteins. J Biol Chem 271, 20235–20237.
Valentin M, Yang E (2008). Autophagy is activated, but is not required for the G0 function of BCL-2 or BCL-xL. Cell Cycle 7, 2762–2768.
Voges D, Zwickl P, Baumeister W (1999). The 26S proteasome: a molecular machine designed for controlled proteolysis. Annu Rev Biochem 68, 1015–1068.
Webb JL, Ravikumar B, Atkins J, Skepper JN, Rubinsztein DC (2003). Alpha-synuclein is degraded by both autophagy and the proteasome. J Biol Chem 278, 25009–25013.
Yamamoto A, Tagawa Y, Yoshimori T, Moriyama Y, Masaki R, Tashiro Y (1998). Bafilomycin A1 prevents maturation of autophagic vacuoles by inhibiting fusion between autophagosomes and lysosomes in rat hepatoma cell line, H-4-II-E cells. Cell Struct Funct 23, 33–42.
Yew EH *et al*. (2005). Proteasome inhibition by lactacystin in primary neuronal cells induces both potentially neuroprotective and pro-apoptotic transcriptional responses: a microarray analysis. J Neurochem 94, 943–956.
Yoshimori T (2004). Autophagy: a regulated bulk degradation process inside cells. Biochem Biophys Res Commun 313, 453–458.
Yoshimori T, Yamamoto A, Moriyama Y, Futai M, Tashiro Y (1991). Bafilomycin A1, a specific inhibitor of vacuolar-type H(+)-ATPase, inhibits acidification and protein degradation in lysosomes of cultured cells. J Biol Chem 266, 17707–17712.
Zheng Q, Li J, Wang X (2009). Interplay between the ubiquitin-proteasome system and autophagy in proteinopathies. Int J Physiol Pathophysiol Pharmacol 1, 127–142.
Zhu K, Dunner K Jr, McConkey DJ (2010). Proteasome inhibitors activate autophagy as a cytoprotective response in human prostate cancer cells. Oncogene 29, 451–462.